ABSTRACT

Title of Document:	COMPARISON OF WASTE HEAT DRIVEN AND ELECTRICALLY DRIVEN COOLING SYSTEMS FOR A HIGH AMBIENT TEMPERATURE, OFF-GRID APPLICATION
	Christopher P. Horvath, Master of Science in Mechanical Engineering, 2012
Directed By:	Dr. Reinhard Radermacher, Professor Department of Mechanical Engineering

Forward army bases in off-grid locations with high temperatures require power and cooling capacity. Each gallon of fuel providing electrical power passes through a complex network, introducing issues of safety and reliability if this network is interrupted. Instead of using an engine and an electrically powered cooling system, a more efficient combined heat and power (CHP) configuration with a smaller engine and LiBr/Water absorption system (AS) powered by waste heat could be used. These two configurations were simulated in both steady state and transient conditions, in ambient temperatures up to 52°C, providing up to 3 kW of non-cooling electricity, and 5.3 kW of cooling. Unlike conventional AS's which crystallize at high temperatures and use bulky cooling towers, the proposed AS's avoid crystallization and have air-cooled HXs for portability. For the hottest transient week, the results showed fuel savings of 34-37%, weight reduction of 11-19%, and a volumetric footprint 3-10% smaller.

COMPARISON OF WASTE HEAT DRIVEN AND ELECTRICALLY DRIVEN
COOLING SYSTEMS FOR A HIGH AMBIENT TEMPERATURE, OFF-GRID
APPLICATION

By

Christopher P. Horvath

Thesis submitted to the Faculty of the Graduate School of the
University of Maryland, College Park, in partial fulfillment
of the requirements for the degree of
Master of Science
2012

Advisory Committee:
Professor Reinhard Radermacher, Chair
Professor Gregory Jackson
Associate Professor Bao Yang

Dedication

To my parents for their unending love, support, and encouragement, to my brother

who has been a fountain of knowledge and wisdom for me, and to my friends in the

Maryland area who have made my experience at the University of Maryland most

enjoyable.

Acknowledgements

I am thankful to all of my officemates both in the compressor lab and the ACTA lab who contributed toward creating a productive, comfortable, cooperative, and fun atmosphere with an international flavor.

I would like to extend my gratitude to all those that I worked with in the Heat Pump Lab for sharing their insight and knowledge into the different aspects of experimental work. Most especially, thanks to Jan Muehlbauer, Daniel Leighton, and Bracha Mandel who have taught me hands-on knowledge in designing and building physical systems. Also, I am continually inspired by their ability to troubleshoot difficulties both small and large.

I am also thankful to all my remaining colleagues in the CEEE who through their conversations and presentations have enhanced my understanding in the field of energy and engineering.

Table of Contents

List of Tables

List of Figures

Nomenclature

Acronyms:

AFR	Air Fuel Ratio
AS	Absorption System
ARTI	Air-Conditioning and Refrigeration Technology Institute
CFM	Cubic Feet per Minute
CHP	Combined Heat and Power
COP	Coefficient of Performance
CPA	Compressor Pressurized Absorber
DB	Duct Burner
ECU	Environmental Control Unit
EES	Engineering Equation Solver
FCC	Fuel Chargeable to Cooling
HX	Heat Exchanger
IC	Internal Combustion
ISHPC	International Sorption Heat Pump Conference
LHV	Lower Heating Value
LMTD	Log Mean Temperature Difference
MIAE	Membrane integrated Absorber Evaporator
MFR	Mass Flow Rate
NC	Non-Cooling
PLR	Part Load Ratio
PMC	Phenylmethlycarbinol
PR	Pressure Ratio
RPM	Rotations per Minute
SHF	Sensible Heat Factor
SSLC	Separate Sensible and Latent Cooling
TRNSYS	a TRaNsient SYstem Simulation program
VCS	Vapor Compression System
VFR	Volumetric Flow Rate

Abbreviations and symbols:

Cons	Consumption
Cp	Specific Heat
dP	Pressure Drop
f	Fraction
Gals	Gallons
Genset	Electrical Generator Set
kPa	Kilopascal
kW	Kilowatt
Q	Heat or energy input
Temp	Temperature
UA	Overall Heat Transfer Coefficient, multiplied by Area
LiBr/Water	Lithium Bromide/Water

Greek Letters:

	Efficiency
	Density

Subscripts:

cool	Cooling
d	Desorber
des	Desorber
DB	Duct Burner
e	Evaporator
Eff	Effectiveness
Elec	Electrical
Exh	Exhaust
Max	Maximum
WH	Waste Heat

Chapter 1: Introduction

1.1 Background

Military applications often differ greatly in requirements from the average conditions that are encountered at home in the United States. Envision for a moment the summer climate of the Middle East where temperatures can rise above 45°C with high humidity. In conditions like these, air conditioning becomes more of a necessity than a luxury for soldier comfort but also for proper electrical equipment function which requires lower temperature and humidity. This has led to a widespread use of environmental control units (ECU), which consist of vapor compression systems (VCS) to cool temporary bases, buildings, and vehicle spaces. However, in an off-grid location, as is typically the case, these ECUs require electrical input which is supplied by diesel powered electrical generator sets (Genset). Unfortunately, the fuel to electricity conversion efficiency of these units is quite low at around 20%, resulting in high costs both in safety and money. A report in 2011 suggested that the military costs of air conditioning were as high as $20.2 billion per year when considering infrastructure, transport, and safety associated with the delivery of fuel [1]. Even if this figure is exaggerated, it certainly does highlight the necessity for energy conservation measures. Each gallon of saved fuel compounds quickly into substantial monetary savings with quick payback, in addition to the greater safety and effectiveness of the military associated with reduced fuel transport. As a result, the military has been interested in technologies that can improve the current situation, while meeting the existing conditions. The contemporary concept of combined heat and power (CHP) is one that could certainly be well applied to such a situation, as it entails

the utilization of both electrical output and waste heat (WH) of a generator in order to improve efficiency while meeting the same needs. The chosen method of WH utilization in this study was to make use of absorption system (AS) technology to provide space cooling.

As an overall metric for cooling technology, coefficient of performance (COP) is often used but would be misleading in this situation. This is because it is not a useful metric for comparing AS's with other cooling technologies since COP does not take into account the source of the input, be it electricity or heat. In its place, fuel chargeable to cooling (FCC) is employed as an alternative metric, described as the amount of cooling divided by the fuel attributed to that cooling. The procedure for its calculation is defined below in Eqs. 1 through 5, and is used as part of the analysis for each investigated system. Hotel power is the amount of non-cooling (NC) electrical load that the engine must provide.

$$Total\ Electrical = Hotel\ power + \frac{Q_{cooling}}{COP_{VCS}} + Parasitic\ Power \tag{1}$$

$$Q_{Fuel\ total} = \frac{Total\ Electrical}{\eta_{elec}} + Q_{DB} \tag{2}$$

$$Q_{Fuel\ for\ non-cooling} = \frac{Hotel\ Power}{\eta_{elec}} \tag{3}$$

$$FCC = Q_{Fuel\ total} - Q_{Fuel\ for\ non-cooling} \tag{4}$$

$$Fuel\ Chargable\ to\ Cooling(FCC)\ Efficiency = \frac{Q_{cool}}{FCC} \tag{5}$$

1.2 Literature Review

CHP systems offer many advantages over conventional electrical production. It can be effectively applied to both large scales such as cities, campuses, or towns as well as to smaller scales such as single family homes or business offices. The obvious requirement though is that there must be a need to utilize the heat in addition to the electricity. One way the heat can be used is to create additional power if the heat is of high enough quality. Alternatively, this heat can be used directly to heat water and circulated to heat a space, or it can be used with a thermally activated cooling technology to provide cooling or air-conditioning. There have been numerous studies investigating the practicality of CHP systems, each targeting a particular application or highlighting a certain technology. Many of these have shown the opportunities for which CHP can be positively applied. For instance, an evaluation was carried out for a district CHP application consisting of a 1 MW solid oxide fuel cell (SOFC) and hot water distribution. The results showed that the two could be sustainably paired together for 500 homes while reducing environmental emissions [2]. Another CHP example investigated the use of an organic rankine cycle (ORC) used for heating in a commercial building for different locations and profiles. When compared with the baseline building model, it showed improvements as high as 30% energy savings, 20% reductions of CO_2, and 19% cost savings, varying by location and corresponding weather conditions [3].

There are a variety of thermally activated cooling technologies available, each offering advantages dependent upon specific applications and waste heat quality. These technologies are able to take advantage of heat sources and deliver cooling by means of chemical processes. A review of these technologies from Deng et al. [4] discusses the

3

technologies with their relative advantages and disadvantages. Included are water/ammonia AS's, Lithium Bromide/Water (LiBr/Water) AS's, adsorption systems, and solid or liquid desiccant cooling systems. Absorption chillers can be designed as single-effect, double-effect, or even triple-effect. While double and triple-effect systems have better performance, their additional complexity and cost often inhibit their practicality for low capacity systems. Thus, for the small scale investigated in this study, a single-effect absorption chiller system was selected for its simplicity and highest practicality.

LiBr/Water AS's can be applied in many contexts, ranging from solar thermal energy, biomass, and chemical/industrial plants, to more conventional CHP situations such as small scale generators and district power with heating or cooling [5]. The advantage of AS's lies in the use of a pump to transfer vapor from low to high pressure instead of using high energy consuming compressors to pressurize vapor. The AS enables this by the chemical properties of the working fluid pair. Since the refrigerant has an affinity to absorb into the absorbent, it can be pumped as a liquid to higher pressure once the heat of mixing has been removed.

An extensive explanation of absorption technology for use in cooling and heating has been written in textbook format by Herold et al. [6]. A simple AS schematic from this textbook is shown below in Figure 1. This diagram shows all of the main components and heat exchangers (HX) associated with the AS. Starting with the desorber, the waste heat is input to the system where water is boiled out of the LiBr/Water solution to point 7. The water vapor which leaves the desorber at point 7 then passes through the condenser to release heat to the ambient, then drops to lower pressure through an expansion valve.

4

At the lower pressure the water passes through the evaporator where the space cooling occurs, and then enters the absorber as vapor. This side of the system is very similar to that of a typical VCS, but since the refrigerant here is water, the temperature of the evaporator must be considered during design such that it does not freeze during operation.
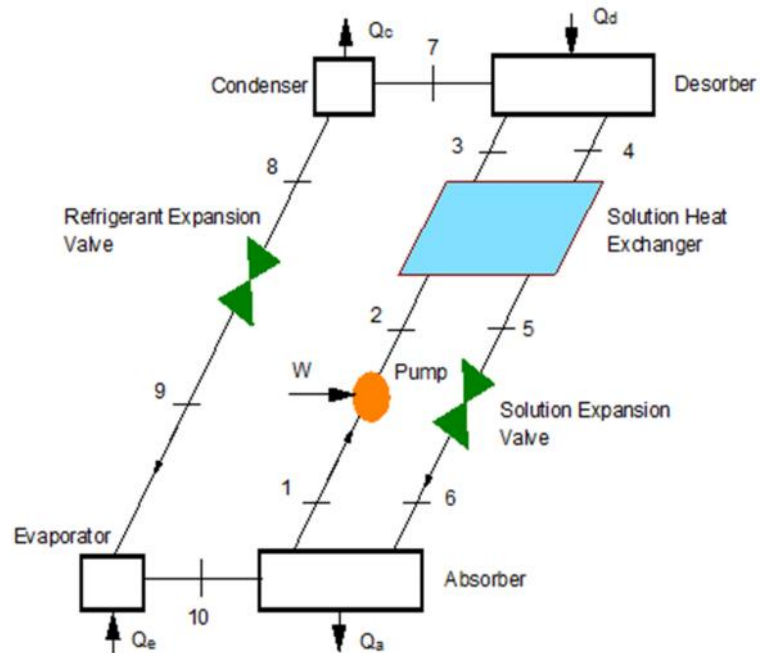
Figure 1: Basic AS Schematic (indicating the main HXs: desorber, condenser, evaporator, absorber, solution heat exchanger, as well as pressure changing devices of pump and expansion valves. Two pressure system, desorber and condenser at high pressure, with evaporator and absorber at low pressure)

The other stream leaving the desorber is the concentrated LiBr/Water solution at high temperature, which passes through the solution heat exchanger to preheat the diluted LiBr/Water stream before it enters the desorber. After the concentrated solution leaves the solution heat exchanger it passes through a valve to bring it to lower pressure as it enters the absorber. At this point, the two streams combine and release heat as the water vapor absorbs into the concentrated solution, becoming a liquid stream leaving the

absorber at point 1. It then is pumped to higher pressure before passing through the solution heat exchanger and then finally arrives back at the desorber.

One of the reasons LiBr/Water absorption technology was chosen for this application is due to a high COP when compared to other thermally-activated cooling technologies. It also does not have the toxicity issues of ammonia/water AS's. However, at high ambient temperatures they suffer from crystallization, limiting their applications to less portable situations with cooling towers to water cool the heat exchangers. Crystallization typically first occurs in the concentrated liquid solution stream at point 6, after the expansion valve and before the absorber heat exchanger. This occurrence results in a degradation of performance and will damage the system over time. Thus, there are great implications with developing anti-crystallization strategies, especially if coupled with air-cooled absorber heat exchangers, as it would enable a release of portable, flexible AS's [7].

1.3 Objectives

The objective of this thesis was to evaluate alternatives and identify the CHP design with the least weight and fuel consumption which provides power and cooling under extreme conditions. The maximum cooling demand was defined as 5.275 kilowatt (kW), while at 51.7°C ambient temperature and 35.2 g/kg humidity ratio. The supply air was also defined as 0.280 kg/s, 525 cubic feet per minute (CFM), including 0.024 kg/s (45 CFM) of ventilation air.

Since the Genset would be an important component in the simulations, it was based upon experimental data provided for this project indicating the performance of a 3 kW diesel

engine as shown in Table 1 [8]. This experimental data was based upon a 3 kW tactical

quiet generator Genset from DRS [9]. This Genset is based upon a Yanmar Diesel, L70,

air-cooled engine [10]. These engine details were useful as the basis for characterizing

the Genset physical information, and the performance of the engine component. The

number of hours per given engine load in Table 1 was used to create one plausible load

profile as shown in Figure 2. The table describes the fuel consumption rate, duration, and

the exhaust temperature for each particular load. This experimental data was used as the

basis for the engine data of the models, scaling for the 5 kW and 10 kW Gensets as used

for the different system models. More details of the engine component are outlined in

Section 4.1.

Table 1: Experimental fuel consumption and load profile for a 3 kW engine

Load [kW]	Fuel Cons [gal/hr]	Fuel Cons [kg/s]	Mission Profile [hours]	Exhaust Temp [°F]	Exhaust Temp [°C]
0	0.103	0.000091	0.00	525	274
0.75	0.180	0.000157	4.60	625	329
1.5	0.224	0.000196	7.25	775	385
2.25	0.281	0.000246	7.25	725	413
3	0.353	0.000309	4.60	850	454
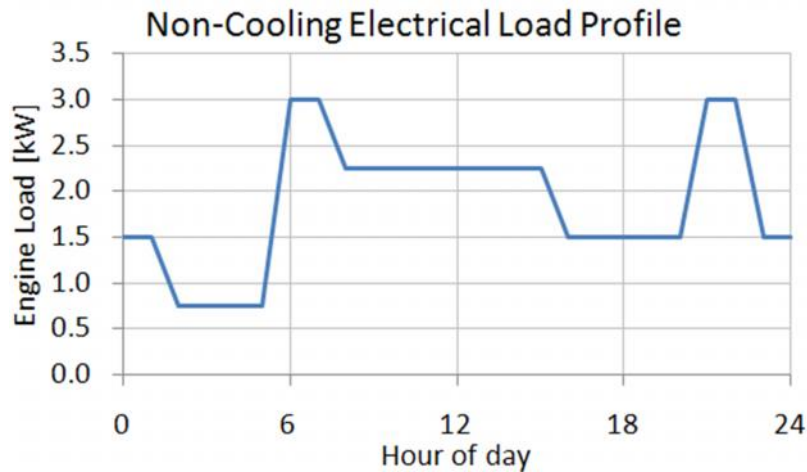
Figure 2: Load profile for non-cooling electrical load (each engine load segment sums to the total durations found in Table 1, in total adding to 24 hours. Engine never runs at 0 kW, idle mode)

7

The required indoor conditions were set based upon a need to keep electronics cool and dry, rather than to provide the most comfortable environment for human occupants. Nonetheless, the environment would certainly be more comfortable than the alternative outdoor conditions. The indoor conditions for the space were therefore set at a temperature of 32.2°C, with a humidity ratio of 15.2 g /kg.

While the design cooling condition was 5.275 kW at 51.7°C and 3 kW of non-cooling electrical load, the cooling load was allowed to vary with the temperature and engine load profiles. Eq. 6 shows the dependence of cooling load on the independent variables and was included in the models to determine the corresponding fuel requirement. The 0.4 kW accounts for the internal heat gain of two occupants, 58.2% of the NC electrical load was dumped into the occupied space by electronic equipment, and the remaining heat load was due to ventilation, infiltration, and conduction loads varying with ambient temperatures. The derivation of this equation is detailed in the Appendix.

$$Q_e [kW] = 0.4 + 0.582 * Hotel\ Power + 0.1605 * (T_{ambient} - T_{setpoint}) \qquad (6)$$

In order to incorporate the cooling load calculation as shown above, a transient weather profile was chosen as close to the design condition as possible. Through the weather database Meteonorm [11], the location of Abu Dhabi in the United Arab Emirates was identified to have high temperature peaks closest to 51.7°C. To meet the design temperature, 7°C was added to the hottest week of the year, August 13th to August 20th, forming the worst week condition. Figure 3 demonstrates the resulting weather profile, reaching peaks of 51.7°C.
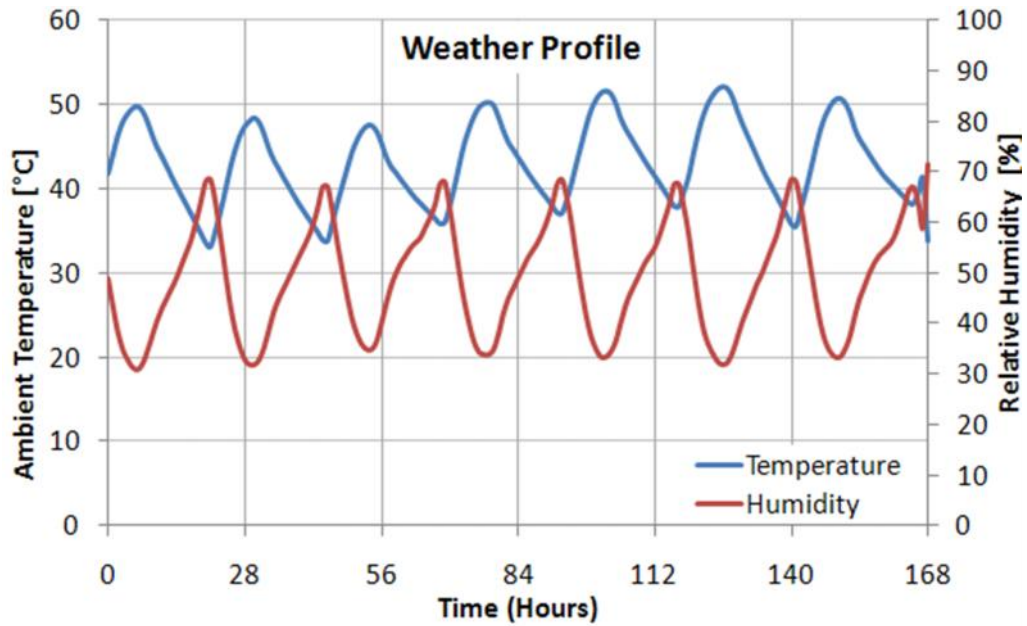
Figure 3: Seven day weather profile for Abu Dhabi, UAE (plus 7°C), corresponding to the hottest week of the year

There were several simulation cases investigated in this study. The first simulation evaluated each system for a one week duration, given a static 51.7°C ambient temperature and supplying 3 kW of hotel power. The second simulation evaluated the systems based on a week of transient ambient temperature, following the weather profile displayed previously in Figure 3, while supplying the hotel power transient profile shown in Figure 2. The third and final simulation evaluated the systems for an entire year with the transient weather profile as shown in Figure 4, and supplying the same hotel power as the second simulation case. While the hottest week had 7°C added to meet the design temperature peak, for the full year evaluation 7°C was added only for the summer months (3,960 to 6,840 hours). Table 2 summarizes the three simulation cases for better clarification.

9
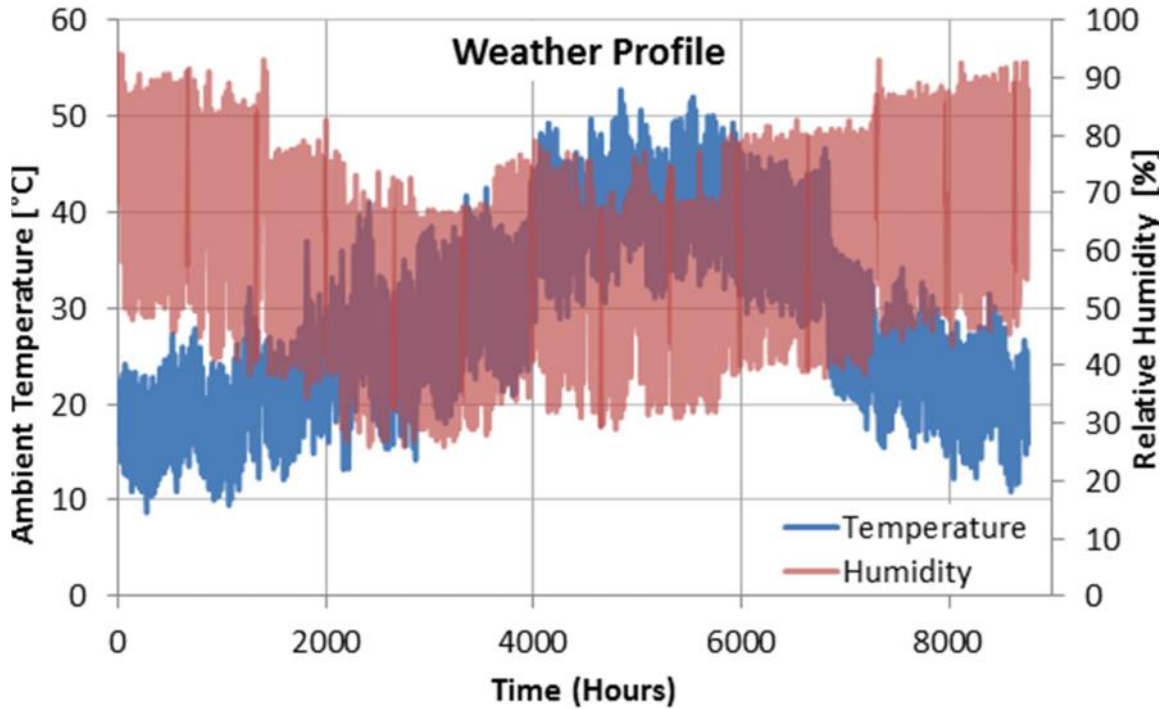
Figure 4: Full year weather profile for Abu Dhabi, UAE (+7°C, between 3,960 & 6,840 hours, corresponding to the summer season)

Table 2: Summary of the three simulation profiles investigated

Simulation #	Duration	Weather Conditions	Hotel Power
1	One Week	Steady State 51.7°C	3 kW
2	One Week	Transient with 51.7 °C peaks	Transient profile 0.75 – 3 kW
3	One Year	Transient with 51.7 °C peaks	Transient profile 0.75 – 3 kW

Since the crystallization issue presents a great disadvantage to this technology, developing various anti-crystallization approaches was one of the important objectives of this work. Many ideas were investigated, including separate sensible and latent cooling (SSLC), a cascaded arrangement, a membrane integrated absorber evaporator (MIAE), a compressor pressurized absorber (CPA), and working fluid additives. These approaches are discussed in detail in Chapter 2.

1.4 Approach

In the effort to compare the proposed systems with the conventional system, two main pieces of software were used for modeling: Engineering Equation Solver (EES) and a TRaNsient SYstem Simulation program (TRNSYS) [12, 13]. EES was used to model the basic VCSs and AS's, containing assumptions pertinent to heat exchangers, flow rates, parasitic loads, and temperature set points. These models were then used to create curve fits based on varying ambient temperature and engine exhaust temperature.

These curve fits were then included in corresponding TRNSYS models to simulate the transient performance of the whole system which encompassed the cooling technology, engine, duct burner (DB), weather profiles, cooling load, and NC electrical load. This configuration provided the most simplistic solving approach with more accuracy, flexibility, and customization than a simple TRNSYS AS model could provide, without the complexity of running EES concurrently with TRNSYS.

1.5 Legacy System Characterization

The first step in determining the advantages of the proposed systems was to identify the characteristics of the system that was currently being used. From the project sponsors it was determined that a 10 kW Genset was the current technology used to meet the maximum NC electrical load of 3 kW, and enough electricity to power the VCS for the cooling needs of the space. It was assumed that its VCS used R134a, and that the evaporator delivered air at a temperature of 5°C. This supply temperature was chosen as it could be used to achieve adequate dehumidification for a typical space. These assumptions in conjunction with those shown in Table 3 result in a COP of 1.06 at the

11

design condition. This equates to about 5.0 kW of electrical load for the desired cooling

demand of 5.275 kW, and results in a total engine electrical load of 8 kW. This result was

considered justified because, if a higher COP were achieved, this would indicate that the

legacy engine was oversized for its purpose.

Table 3: Legacy VCS assumptions and characteristics

	Conventional VCS
Evaporator approach temperature	7°C
Condenser approach temperature	5°C
Superheat	10°C
Subcooling	5°C
Compressor isentropic efficiency	0.61
Compressor motor efficiency	0.85
Evaporator air inlet	38.9°C
Evaporator air outlet (T, RH)	5°C, 100%
Condenser air/water inlet	51.7°C
dP in evaporator (refrigerant)	50 kPa
dP in condenser (refrigerant)	100 kPa

The modeling of the legacy VCS was done in EES to find a COP curve fit for

incorporation in the TRNSYS model. This COP curve fit is shown in Figure 5, using

TableCurve 2D software [14]. For a better understanding of the legacy system, a

schematic with its components is given in Figure 6.
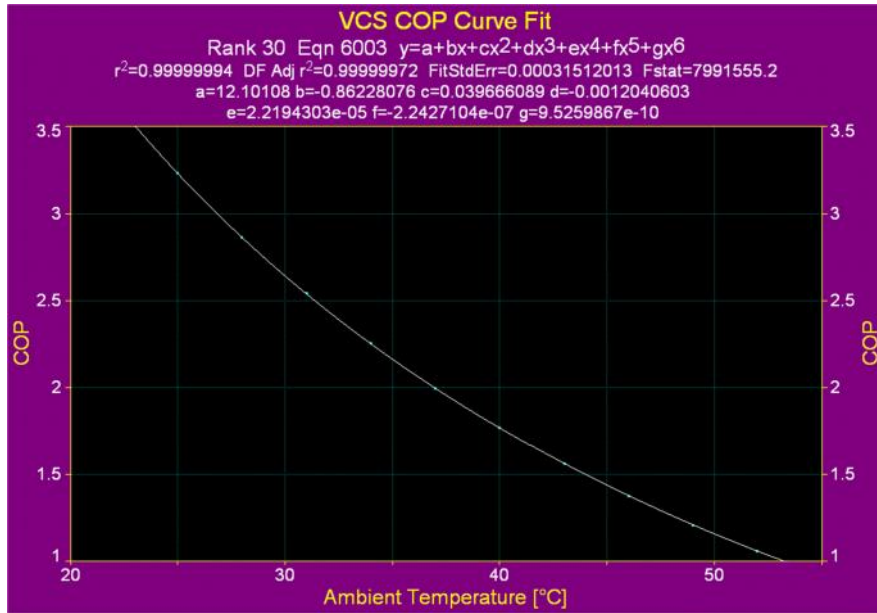
Figure 5: VCS Curve fit for legacy system VCS, with 5°C evaporator temperature (design point temperature has a COP of 1.06, and a COP as high as 3.25 at 25°C)
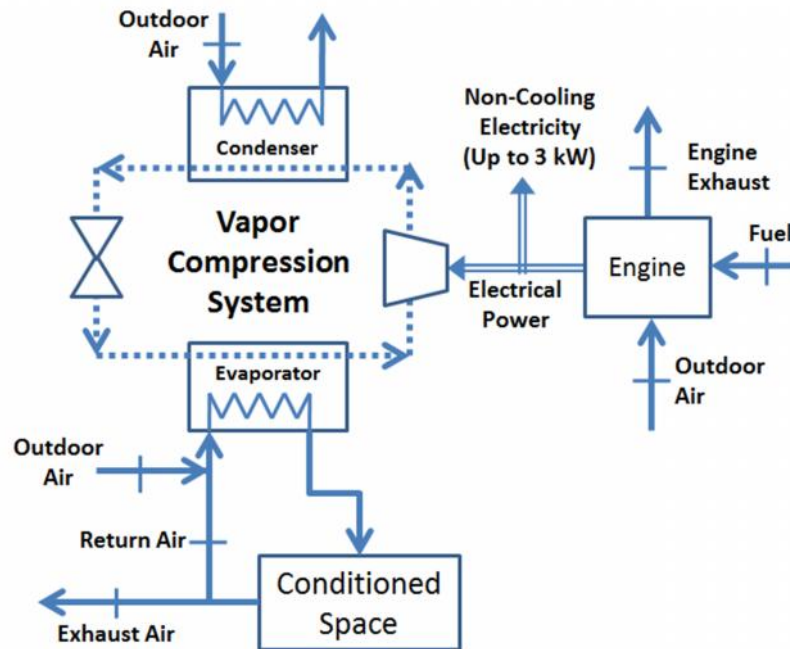
Figure 6: Schematic of legacy system components (main items include engine, conditioned space, and VCS components: compressor, condenser, evaporator, and expansion valve. Engine powers both the VCS and up to 3 kW of NC electricity)

The FCC was calculated for the legacy cooling system as previously discussed in Section 1.1, resulting in a FCC efficiency of 0.225. This provides a useful metric with which to

compare the proposed systems. The volume and weight of the legacy system was determined by the summation of the weight of the 10 kW Genset and a VCS system capable of handling the cooling load. Consisting of a 10 kW Genset from DRS power solutions [15], and a 6 kW ruggedized military VCS manufactured for operation at 120°F (48.9°C) by AirRover [16], the total weight without fuel summed to 649.4 kg, with a volume of 1.82 m^3. Details of the weight/volume constituents for the legacy system are provided in Section 5.1, including the weight and volume of the fuel.

Chapter 2: Crystallization Approaches

2.1 Crystallization Characterization

Before investigating specific anti-crystallization approaches, it was first necessary to characterize the phenomenon with LiBr/Water in order to understand how different approaches would affect the situation. A good way of visualizing this was to plot the solubility limits as done by Gluesenkamp et al. [17], using data of LiBr solubility in water from Boryta [18]. This data was plotted on a Dühring chart with a superimposed absorption cycle. This diagram is shown in Figure 7.
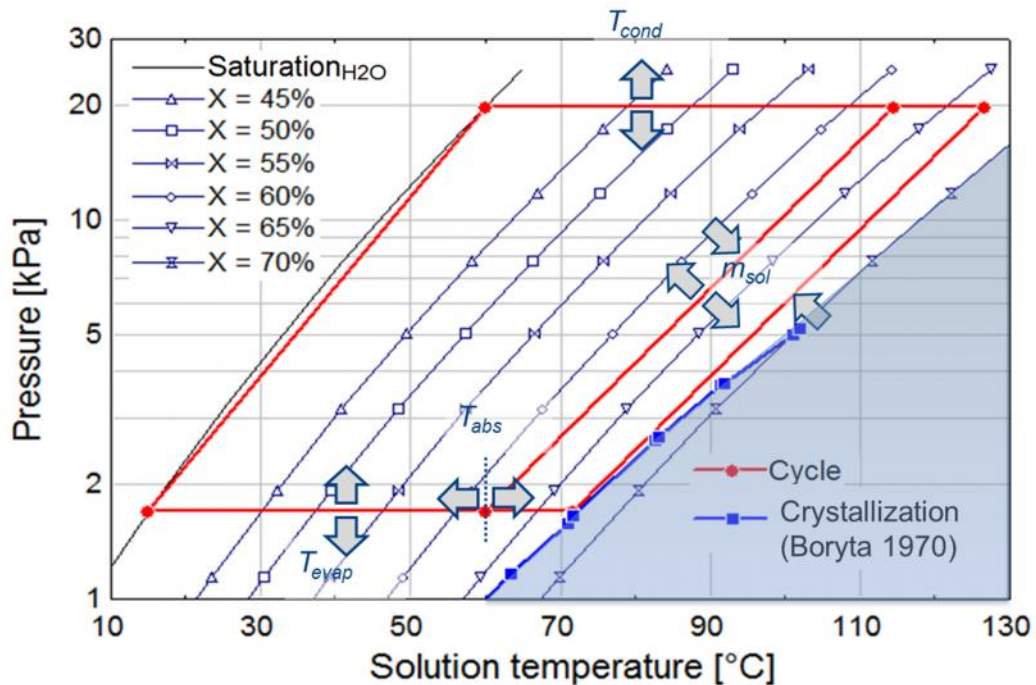
Figure 7: Water/LiBr Dühring chart with absorption cycle, (cycle indicated in red, crystallization region at bottom right, and AS characteristics indicated by arrows. Raising evaporator or absorber temperature results in moving away from crystallization)

This diagram is useful in a number of ways as it demonstrates how the operating conditions affect and move the cycle. Firstly, it can be seen that according to the

diagram, the location where the crystallization is most likely to occur is in the bottom right, or in a physical sense, at the point where the concentrated solution exits the expansion valve, before entering the absorber heat exchanger. One of the affecting parameters is the temperature of the evaporator. As the evaporator operates at a higher temperature and consequently higher pressure, the absorber pressure follows suit to operate at a higher pressure. This effectively raises the AS out of the crystallization region. Additionally, the absorber temperature also has a great impact upon the crystallization of the unit. If the absorber temperature is lowered, then it tends to pull away from the crystallization region, but if the temperature rises, as is the case with higher ambient temperatures, then it moves towards the danger of crystallization. The difference in concentration between the concentrated and dilute solution streams is what the X represents, bringing the two parallel lines either closer together or further apart.

2.2 System Modifications

2.2.1 Compressor Pressurized Absorber

One of the methods considered was to increase the pressure of the absorber, disjoining it from the evaporator pressure [7]. This would be achieved by placing a compressor between the evaporator and the absorber as demonstrated by the cycle diagram in Figure 8 below. Figure 9, which follows demonstrates on the Dühring plot what effect the compressor would have. It can clearly be seen how this would benefit the system in moving away from the crystallization region. Preliminary modeling in EES showed that it would only require a small electrical power of 250 Watts at the design point to cover the pressure ratio of 2.3.
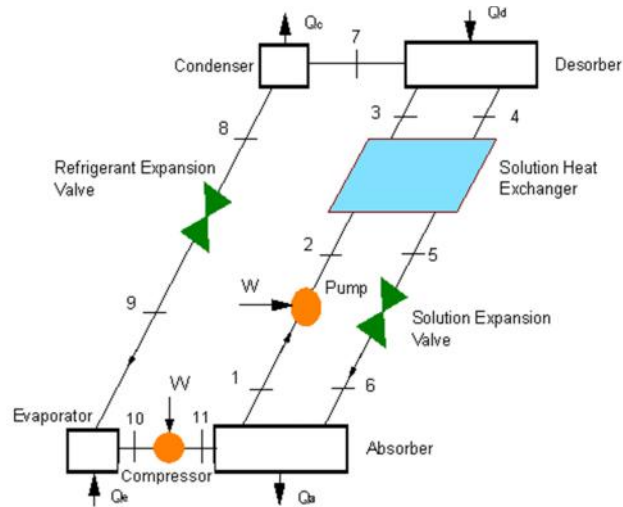
Figure 8: AS diagram with compressor pressurized absorber (CPA) strategy (compressor is placed between the evaporator and absorber units to raise absorber pressure)
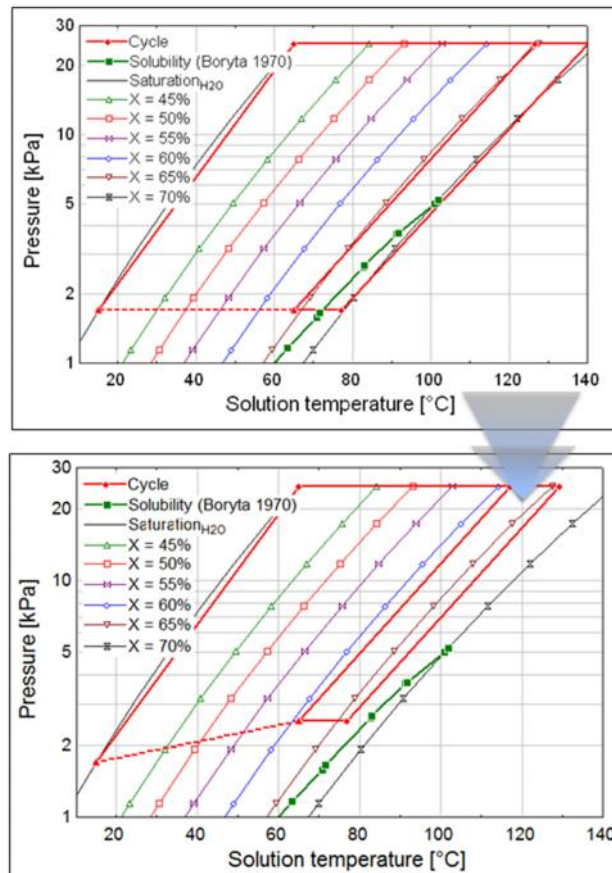
Figure 9: Dühring representation of CPA strategy (by placing the compressor between the evaporator and absorber the cycle is theoretically able to be removed from crystallization region)

Despite its original promise, this approach turned out not to be particularly feasible for this application. A variety of options were investigated which included axial fans, centrifugal type compressors, diaphragm pumps, and oil-free screw and lobe type compressors. However, given the capacity of the AS, the low flow rates coupled with the low density made it very difficult to find a suitable match. For example, research from the Air-Conditioning and Refrigeration Technology Institute (ARTI) discussed the implementation of water vapor compression utilizing multistage axial compression and centrifugal compression. It was determined that the latter was more feasible, and identified possible models. However, the application was for a larger pressure ratio, higher capacity system, and would be oversized in specifications as well as in physical size for this application [20]. Consequently, this approach was not pursued further.

2.2.2 Cascaded VCS Configuration

Another approach required the use of a small supplemental VCS [19]. By including the small VCS in a cascaded configuration between the AS and the conditioned space, the VCS could be turned on at the high ambient temperatures to avoid crystallization. While it would increase the cooling load of the AS evaporator slightly, it would allow the AS evaporator to operate with a higher temperature, resulting in a higher pressure through the evaporator and absorber. This is because the VCS is able to deliver the lower temperature required to sufficiently cool and dehumidify the supply air for the space. Including the additional VCS required a chilled water loop between the AS evaporator and the VCS condenser, along with a pump to circulate the chilled water. It also included a bypass loop so that the VCS can be shut off in lower ambient temperatures, with an extra evaporator coil included for cooling the supply air. Figure 10 illustrates this setup with

18

the AS in conjunction with the supplemental VCS. This approach appeared to be practical, and was chosen to be modeled in greater detail.
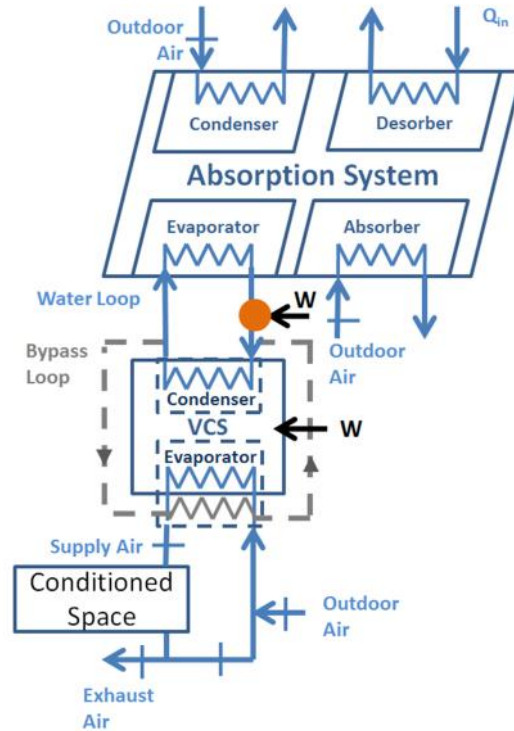
Figure 10: AS schematic with cascaded VCS approach (VCS is placed between the evaporator and conditioned space to raise the AS evaporator temperature and pressure, thus avoiding crystallization)

2.2.3: Separate Sensible and Latent Cooling Configuration

A similar anti-crystallization approach also utilized a small supplemental VCS, but in a SSLC configuration. Such a strategy would allow the AS evaporator to carry out primarily sensible cooling on the large return air stream and small outdoor air stream. This keeps the AS evaporator at a higher temperature and pressure, thus avoiding the crystallization region for the absorber. This would require a split evaporator unit with parallel air channels to enable two streams of cooling, one sensible and one latent. After passing over the AS evaporator, the small outdoor air stream would then be over-cooled

by the VCS evaporator to achieve the desired dehumidification.   There is also an advantage achieved by placing the VCS condenser in the return air stream, in that the VCS can operate with a higher COP than if the condenser were placed in the hot outdoor air. This effectively keeps the power requirement low for the VCS. A flow diagram of the SSLC approach is shown in Figure 11. As can be seen, the ventilation air makes up about 10% of the total air flow, passing first through the AS evaporator and then through the VCS evaporator to a low temperature achieving latent cooling. The return air from the space at a temperature of 32.2°C is used to cool the VCS condenser before an amount equivalent to the ventilation air is exhausted. The remaining air then passes through the AS evaporator for sensible cooling before combining with the ventilation air which together are then supplied to the space.
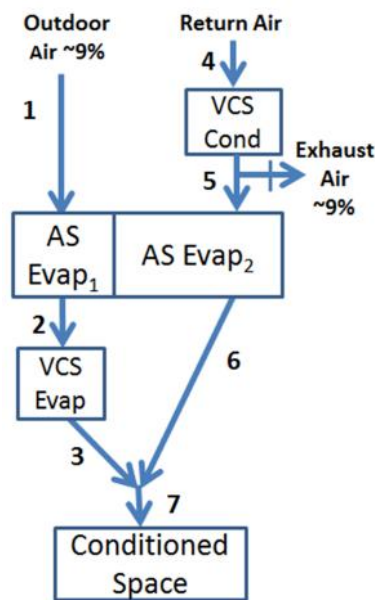
Figure 11: SSLC approach (A split AS evaporator allows for two separate streams, one for the larger, sensible stream to be cooled, and latent cooling for the other, smaller outdoor air stream)

This approach seemed to be rather promising and was investigated for its practicality in avoiding the crystallization limit. Before integrating the SSLC strategy fully with the rest of the system, it was first run at the design condition to see the potential savings. The independent and dependent variables could have been chosen in a few ways, such as either choosing to manipulate total flow rate or the ventilation flow rate. The independent variables which were chosen included the inter-evaporator temperature (points 2 and 6 leaving evaporator) and the total air flow rate. The dependent variables included the VCS load, VCS evaporator temperature, VCS COP, temperature leaving the VCS condenser, and total AS evaporator load. The amount of ventilation air which was solved for had to be monitored to ensure that it was at least meeting the minimum requirement for the space. While placing the VCS condenser in the return air stream presented an advantage in terms of COP, it also linked the AS and supplemental VCS in such a way that required more acute control. For example, when the AS evaporator temperature was raised to avoid crystallization, it increased the load on the VCS evaporator, which in turn raised the temperature of the return air stream leaving the condenser, in turn further affecting the load of the AS evaporator. Therefore, substantial iteration was required in order to find an operating point which provided the correct amount of ventilation, adequate latent and sensible cooling for the space, and a proper margin for crystallization. Eventually, a point which satisfied all of the conditions at a temperature of 51.7°C was unable to be found, and a simulation was run instead for a temperature of 49°C. The full details of the study were reported in a conference paper for the International Sorption Heat Pump Conference (ISHPC) [17].

The study was a steady state analysis comparing a 3.5 kW Genset with AS incorporating SSLC against a 6 kW Genset with VCS. The resulting values of the SSLC configuration showed 22°C and 14.4 g/kg humidity ratio at point 7, a VCS COP of 2.91, VCS compressor power of 446 W, and 882 m^3/hr (525 CFM) of total air flow rate. The major characteristics of the two overall systems are summarized in Table 4. The results of the study are shown in Table 5. The results show the AS in two cases, one where it runs only on heat supplied by a duct burner, and the other in which waste heat is also utilized. The outcome was that using an AS with and without the waste heat results in savings of 11.5% and 2.8% respectively. However, this is only for the design condition and does not take into account parasitic loads of the AS, does not consider actual Genset models, and has not investigated the weight and volume criteria.

Table 4: Characteristics of 6 kW Genset with VCS system and 3.5 kW Genset with AS in SSLC configuration

System Configuration	AS Cooling Capacity	VCS Cooling Capacity	VCS COP	VCS Compressor Power	Engine Size
Conventional	N/A	5.3 kW	1.8	3.0 kW	6.0 kW
Absorption with SSLC	5.6 kW	1.3 kW	2.9	0.45 kW	3.5 kW

Table 5: Fuel consumption results of VCS based system and absorption based system

System Configuration	Engine Size	Cooling Unit	Additional Components	Engine Fuel Cons [g/s]	DB Fuel Cons [g/s]	Total [g/s]
Conventional VCS	6.0 kW	VCS	N/A	0.607	0	0.607
Absorption w/ waste heat	3.5 kW	Absorption w/ SSLC	Duct Burner	0.360	0.177	0.537
Absorption w/out waste heat	3.5 kW	Absorption w/ SSLC	Duct Burner	0.360	0.230	0.590

There was a narrow window within which this system would operate, namely inter-evaporator temperatures between 23 and 25°C. While this method does offer a unique approach to the objectives presented, a more detailed control mechanism and sensitivity

study of the interrelated variables and would have been required. Consequently, this particular configuration was not pursued further for transient study in this work.

2.3 Chemical Additives and Other Approaches

Using additives has been researched as a popular avenue toward avoiding crystallization since the beginning of AS's. An extensive literature review on the most prominent additives for Water/LiBr systems was presented at the 2011 ISHPC [21], which covered many of the possible options that were considered. This review highlighted two particularly promising options. First was 1-nonylamine with ethylene glycol and second was to use a quaternary salt solution consisting of LiBr, $LiNO_3$, LiI, and LiCl [22, 23, 24]. The ethylene glycol would act as a crystallization inhibitor, while 1-nonylamine would enhance heat and mass transfer to reduce the effects of the higher viscosity of the ethylene glycol. In the case of the quaternary salt, the $LiNO_3$ and LiI would act as crystallization inhibitors while the vapor pressure depression caused by these two salts would be mitigated by the fourth salt, LiCl.

Related to the 1-nonylamine mass and heat transfer enhancer, is the Carrol solution originally developed by Carrier. Their solution consisted of LiBr, water, ethylene glycol, and a heat and mass transfer additive. The heat and mass transfer additive was either phenylmethlycarbinol (PMC), or 1-nonylamine. An investigation of Carrier's report on the subject from 1984 reveals that it was likely not PMC. In fact, the use of PMC resulted in a significant performance deterioration, which chronically affected the machine despite attempts to flush and clean it. The 1-nonylamine was determined to be more effective, despite its creation of an oily/greasy sludge-type substance [25].

Interestingly, there were various review articles such as that of Zogg et al. [19] which referenced this Carrier work in support of PMC as an optimal additive for heat and mass transfer, and the key to anti-crystallization approaches.

Relevant to the quaternary salt approach, an actual commercial absorption chiller was found making use of an anti-crystallization additive [19]. The item is the Yazaki ACH-8, a 28 kW system with a patented solution of LiBr/LiCl/LiNO$_3$. According to the paper from Zogg et al. [19], it should operate up to 109°F (42.8°C) as its maximum ambient temperature, however it suffers from a performance decrease of 52% at this point. Yazaki sells approximately two to three units per month, and only offers warranties to customers in Japan. Further investigation of this product led to the patent details, which revealed the mixture ratio by weight as 0.375-0.425:0.225-0.275:1 for LiCl:LiNO3:LiBr. Interestingly, the legal status of this patent seemed to indicate that it was rejected and also expired [26]. This means that it could potentially be used for these purposes without any legal difficulties.

One other commercial product relevant to addressing crystallization was identified from Spanish manufacturer Rotartica, who made a 4.5 kW, single-effect, air-cooled AS unit, model 045v, for use in conjunction with a solar system to provide the heat to power the AS. Through mechanical means, it was able to enhance mass transfer by rotational forces allowing it to operate up to 105 or 115°F without crystallization. Figure 12 shows a cross-section of the technology indicating the operation as the HXs would rotate around the central axis. Unfortunately, this company is no longer in business and the product is not currently available [27].
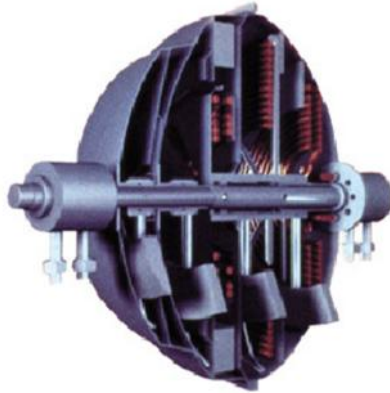
Figure 12: Cut-open view of Rotartica 045V AS [27] (Demonstrating the HXs as they would rotate around the axis to enhance mass transfer and avoid crystallization)

Lastly, a crystallization technique was developed by the project sponsors. This method incorporated a Membrane Integrated Evaporator Absorber (MIAE) unit into the AS. By means of a special membrane and a proprietary design, the unit could operate at different conditions than would a typical evaporator absorber unit found in a conventional AS. However, the evaporator and absorber units needed to be water cooled, and thus incorporated additional water loops, pumps, and air-cooled heat exchangers. This approach was chosen to be modeled in detail as a practical means to avoid crystallization.

Chapter 3: Modeling in Engineering Equation Solver

EES was used to model both cooling technologies which were investigated in this study. This began with a baseline AS which did not incorporate a crystallization strategy, and then was adapted to incorporate the cascaded approach and the MIAE. Additionally, EES was used to model the legacy system VCS, and the VCS for the cascaded system.

3.1 Baseline AS Model

The baseline AS was developed in EES starting with a basic model from Chapter 6 of Absorption Chillers and Heat Pumps [6]. This model described a single effect, water-cooled AS. For this application, instead of using water-cooled HXs with generic sources of heat and heat sinks, the model was adapted more specifically to real conditions. This included adapting the desorber to directly exchange heat with engine exhaust and changing the HXs to be directly cooled by air instead of by refrigerant as currently available in conventional AS's. In particular, this is uncommon, as AS's are typically made for larger capacities than the 5.275 kW of this case and coupled with cooling towers for the absorber and condenser. This adaptation therefore models a more mobile, lighter, AS unit than current options available.

In the evaluation of the various heat exchangers, the overall heat transfer coefficient multiplied by area (UA) values were specified, allowing calculation of the log mean temperature difference (LMTD) and HX heat loads. This was modified for the purposes of primarily air-cooled heat exchangers, with the absorber and evaporator heat exchangers releasing heat directly to the air, and the evaporator directly cooling the air

provided to the space. Additionally, the desorber absorbs heat from engine exhaust as its source. The engine exhaust alone was determined to be incapable of supplying the necessary heat to completely power the AS at the design condition. At the design point, the AS desorber could process about 4 kW of heat from the engine exhaust stream and supply just 2.3 kW of cooling by the evaporator at the design point. Therefore, it was necessary to include a DB in the design to supply the additional heat necessary at the higher ambient temperature. A module was included in the EES file to process the exhaust stream and add the necessary heat by burning fuel directly.

There are a number of advantages to using a DB in this situation, such as better control and good efficiency of direct heat production from fuel. An appropriate DB model was identified from Wayne Combustion Systems [28] to be used in this configuration. The proposed model is MSR-DC: single stage duct burner, fuel pump runs at 3450 rotations per minute (RPM), 3 gallons per hour maximum of fuel consumption, turndown capable, 25 pound weight, with max voltage and current at 12 volts and 5.2 amps respectively. Figure 13 shows a basic flow diagram of the AS with the main components and heat exchangers.
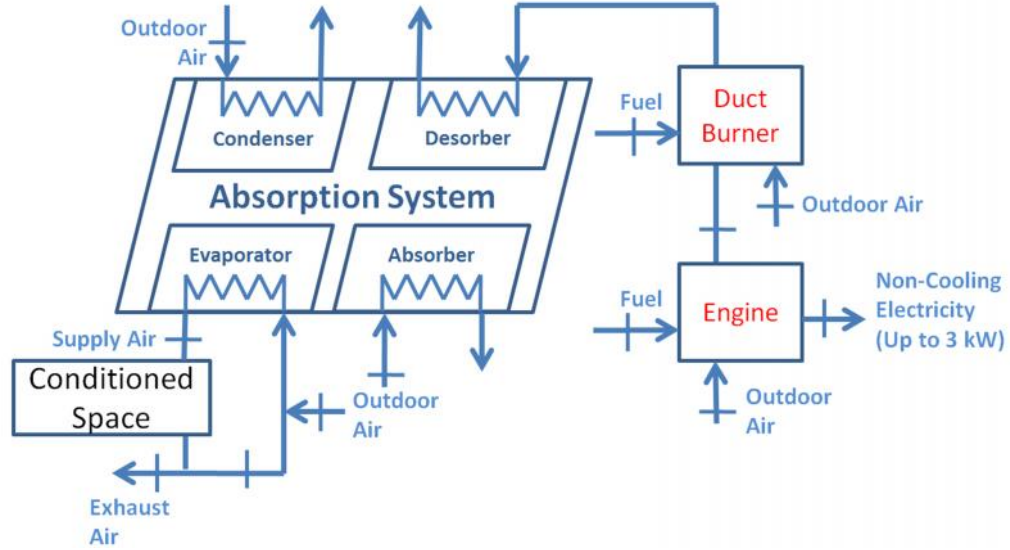
Figure 13: Basic AS schematic (in addition to the AS components, included are the engine and duct burner components)

The water-cooled AS model was adapted to the air-cooled version by adjusting certain parameters. This included lowering the UA to values more plausible for air-cooled heat exchangers. The UA value of the desorber in particular had to be set such that the exiting temperature of the exhaust would not go below the acid dew point. The acid dew point had been determined as around 120°C, and so the temperature leaving the desorber was set to not go below 135°C. The resulting UA values and heat exchanger effectiveness (eff) for each of the EES AS models are shown later in Table 12. The effectiveness of each HX is defined as shown in Eqs. 7 and 8, derived from Chapter 4 of Herold et al. [6] for counter flow HXs. Figure 14 displays the main components and state points of the AS as detailed in EES.

$$HX_{eff} = \frac{Q_{Actual}}{Q_{Max}} = \frac{Q_{Actual}}{(m*C_p)_{Min}*(T_{hot\,side\,inlet} - T_{cold\,side\,inlet})} \qquad (7)$$

$$HX_{eff} = \frac{T_{cold\,side\,out} - T_{cold\,side\,inlet}}{T_{hot\,side\,inlet} - T_{cold\,side\,inlet}} \qquad (8)$$
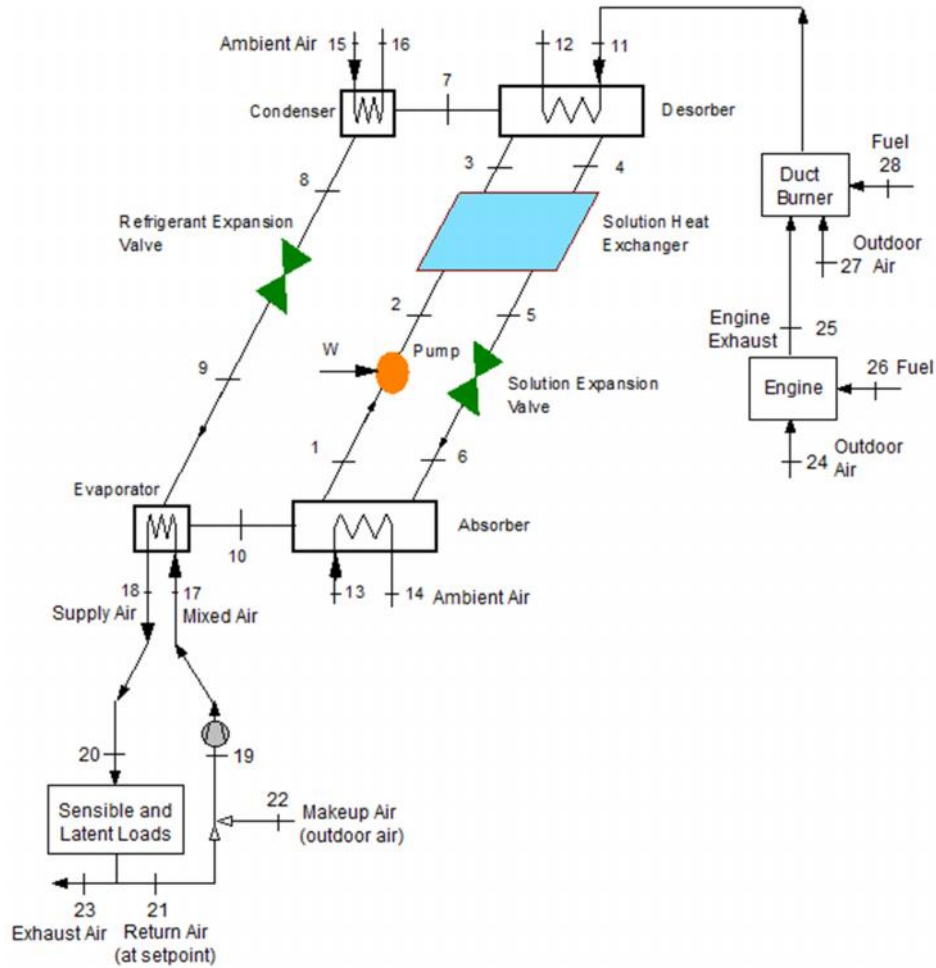
Figure 14: Baseline AS schematic with state points as detailed in EES

A number of inputs to the system were set including the main independent variables of ambient temperature and engine exhaust temperature, and additional static variables of evaporator temperature outlet, space temperature set point, absorber air flow rate, condenser air flow rate, and flow rate of diluted solution through the pump. These inputs are laid out in Table 6.

Table 6: EES inputs for AS model

Criteria	Value
$T_{ambient}$	25 – 51.7 °C
$T_{exhaust}$	329 – 454 °C
T[18]	19°C
$T_{set\ Space}$	32.2 °C
m[1]	0.030 kg/s
m[13]	0.45 kg/s
m[15]	0.3 kg/s

Additionally, the DB can either be specified as on or off for the system, thus there were two different ways in which the model was solved. For the case with the duct burner off, the desorber input was determined by the specified engine exhaust temperature, and the cooling load at the evaporator was solved for. This showed that only 2.3 kW of cooling could be provided by the AS at the design condition using only the engine exhaust, and therefore the heat input would need to be supplemented by a duct burner. Therefore, in the model with the duct burner on, the evaporator capacity was specified by Eq. 6 with the duct burner heat load solved for as approximated by Eq. 9.

$$Q_{desorber} = Desorber\ Effectiveness * (Q_{exh} + Q_{DB}); \tag{9}$$

In each of these cases, a COP was calculated without consideration of the corresponding fuel input. This is helpful in understanding why the COP differs for cases of duct burner on and duct burner off, due to the solving method and varying conditions. This is the motivation for using FCC as a more useful metric to understanding the cooling system. Nonetheless, the COP was still useful as a metric specific to the AS, and was required later in the TRNSYS models to represent the AS.

Parasitic loads were also calculated in EES, which included items such as fans and pumps. These values are reflected in the EES curve fits, and the details pertinent to the

baseline AS parasitics are detailed in Table 7. In order to get a good estimate of the parasitic power requirement, comparable manufactured fans and pumps were found for most components which closely matched the required flow rates. Their maximum flow rates and rated power consumption were identified and then were scaled according to changes in flow rates. The parasitic load for the pump was estimated based upon a manufactured item from Grundfos as an example. Figure 15 is a diagram representing the locations of the parasitic loads indicated by a blue color, both fans and pumps. Point 27 indicates an introduction of outside air if the temperature leaving the duct burner would be too hot, but the temperature stays within a reasonable range for the desorber to handle. However, the fan power was still included. Most values were static, but a few changed with the given conditions. The duct burner pump power for example, was modeled to use its full rated power of 150 W at the maximum condition and use 0 W of power in cases where the duct burner was off. This accounts for most of the slope in the parasitic load curve fit. Other variations came from small variations in flow rates. The size of the Grundfos pump was estimated based on its picture since actual specifications were unable to be found. The choice of fan for the desorber was based on the calculation shown in Eq. 10. Conservative values were assumed for isentropic efficiency, motor efficiency, and pressure drop across the fan as 0.7, 0.5, and 69 kilopascal (kPa), respectively. Its weight and size were then estimated by assuming the same envelope as the makeup air fan from manufacturer Panaflo. Together, the parasitic components sum to a weight of 9.56 kg, and a total of 482 watts, discounting the DB pump power.

$$Work = \frac{\dot{m}*dP}{\rho_{air}*\eta_{isentropic}*\eta_{motor}} \tag{10}$$
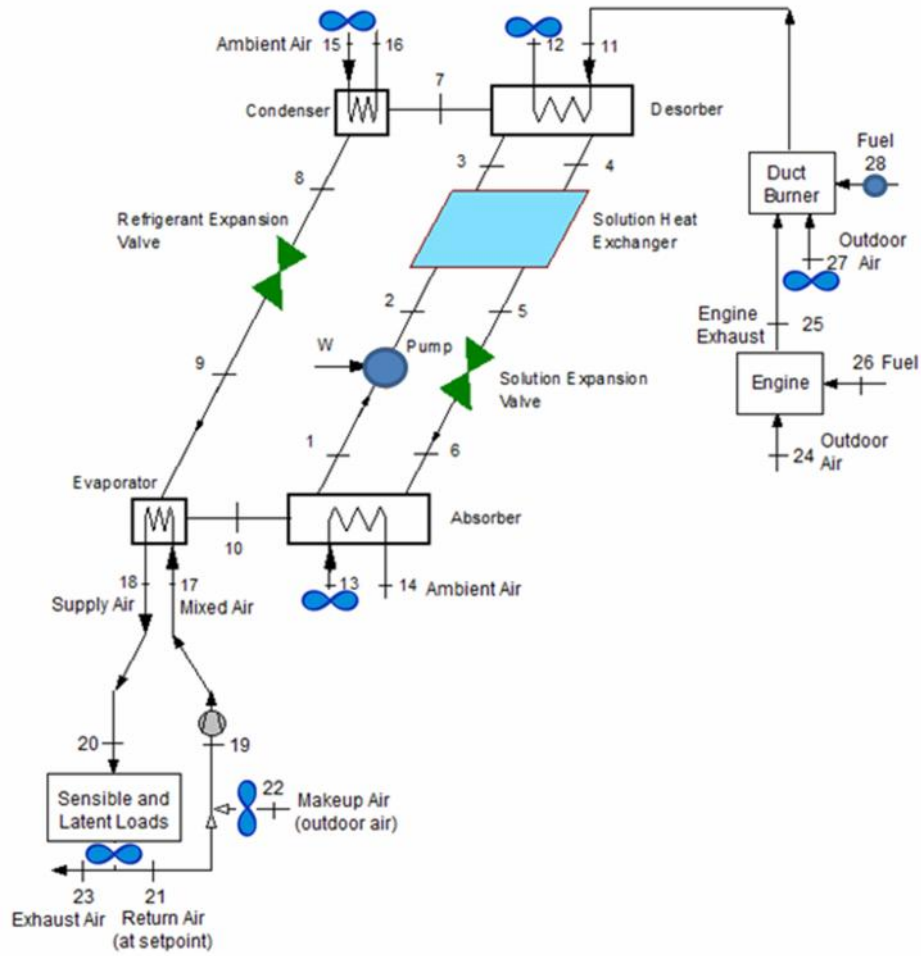
Figure 15: Locations of parasitic loads (in blue) of baseline AS (pump located between absorber and solution HX, fuel pump for DB, fan for conditioned space air return, fan for ventilation air, fans to force convection for absorber and condenser, fan to pull exhaust air through the desorber, and fan to introduce extra air to the DB when air is too hot)

Table 7: Parasitic loads of fans/pumps for baseline AS [29-33]

Parasitic Loads	Manufacturer	Model	Weight [kg]	Size [m³]	Parasitic Electricity [W]
Makeup Air Fan	Panaflo	FBA09A12V	0.40	2.15E-04	4.80
Return Fan	Suncourt	DB208	1.36	6.59E-03	82.50
Condenser Fan	Suncourt	DB210	2.04	1.03E-02	165.00
Absorber Fan	EBM Papst	W2E250	1.81	6.25E-03	175.00
Duct Burner Fan	Sanyo Denki	109P0412H602	0.40	3.52E-05	1.32
Solution Pump	Grundfos	Alpha	3.15	2.83E-02	45.00
Desorber Fan	Theoretical Calc		0.40	2.15E-04	8.29
Sum			9.56	0.02360	481.91

Data was collected from the EES models and fitted to equations using TableCurve 3D [34]. Various curve fits from the EES models were used in TRNSYS and the ones pertaining to the baseline AS are detailed in Figures 16 – 20, with the corresponding equations located in the Appendix as Eqs. 47-51, respectively. These include curve fits of COP, temperature entering the desorber, and parasitic power, which were all later included in the TRNSYS model.
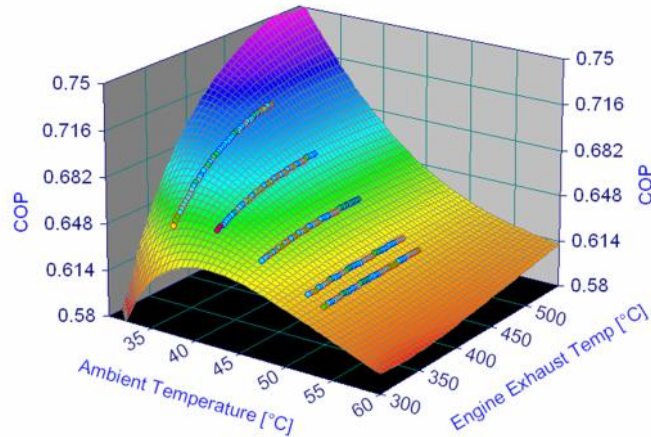
Figure 16: Baseline AS COP curve fit for duct burner on (COP is highest when the ambient temperature is low with high waste heat temperature, and lower with higher ambient temperatures)
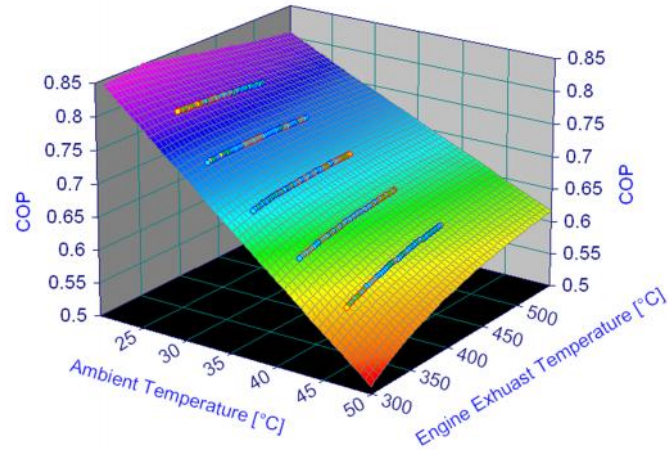
Figure 17: Baseline AS COP curve fit for duct burner off (COP as high as 0.8 for lower ambient temperatures, dipping down to 0.55 with higher ambient temperatures, fairly steady for the varying exhaust temperature when the DB off)
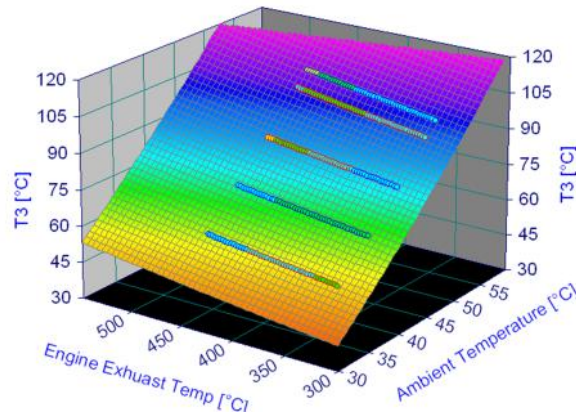
Figure 18: T_3, solution temperature entering desorber for baseline AS (used to model the desorber HX in TRNSYS)
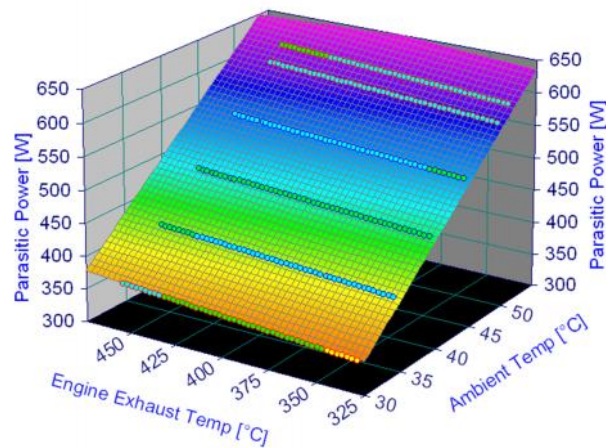
Figure 19: Baseline AS parasitic power curve fit for duct burner on (large variations due to the DB fuel pump running at full power at highest ambient temperature and off at lowest temperature)
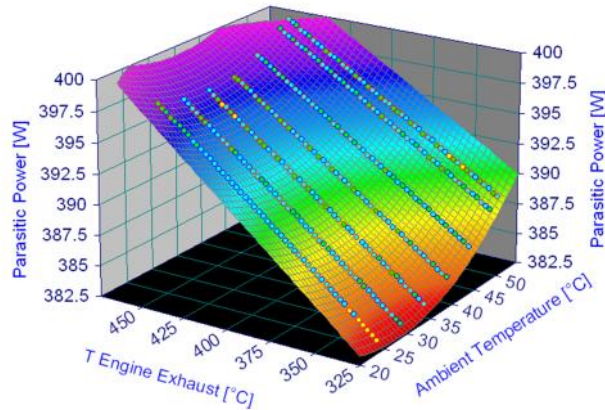
Figure 20: Baseline AS parasitic power curve fit for duct burner off (small change in parasitic loads due to small changes in fan speed and power)

3.2 Cascaded AS Model

The baseline AS EES model was modified to include the cascaded configuration of the VCS with the AS evaporator. Unlike the baseline system, the cascaded system has a control strategy to address the crystallization issue for this particular application. Figure 21 shows the schematic from EES which outlines the additional components in this model. Instead of the liquid-to-air heat exchanger as in the baseline model, the cascaded configuration required a liquid heated evaporator to account for the water loop connecting the AS evaporator with the VCS condenser. This was achieved by changing the UA value of the evaporator to 2.25 kW/K, a more appropriate value for a refrigerant-to-refrigerant HX.
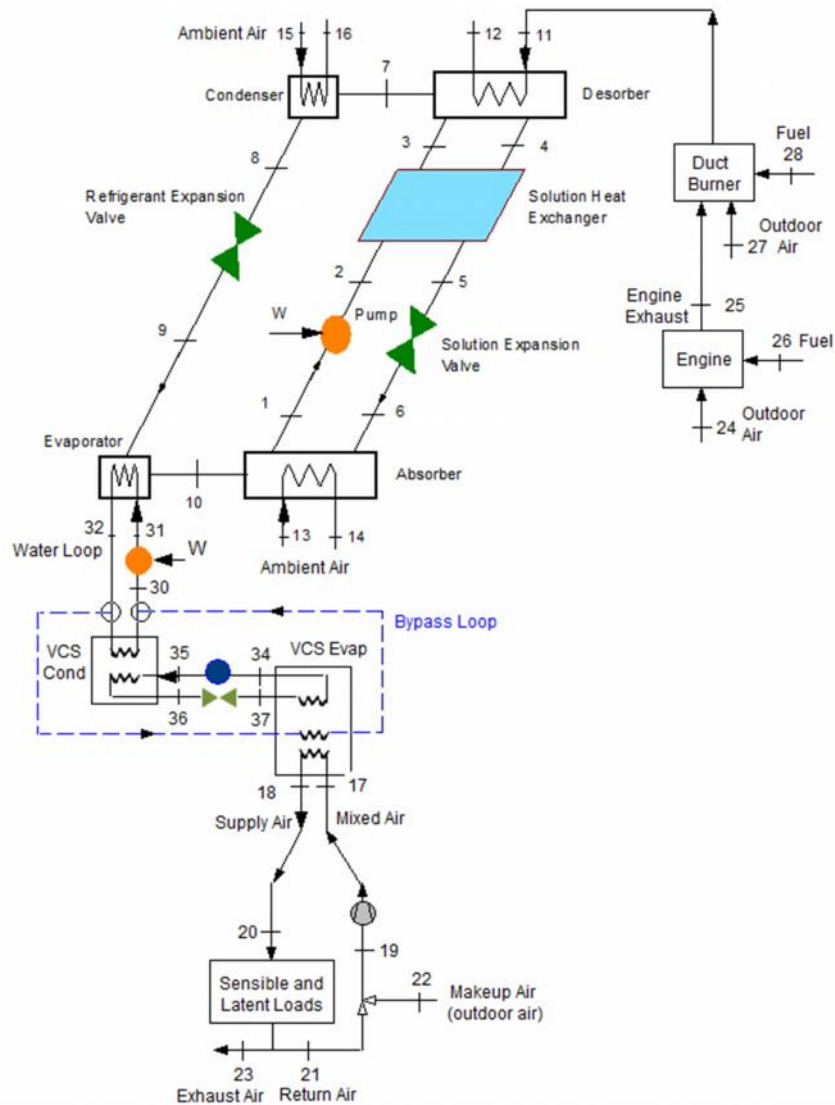
Figure 21: EES schematic of cascaded AS with state points (located between the AS evaporator and the conditioned space is the supplemental VCS. In dotted blue, the bypass line is represented allowing the VCS to be shutoff and allow the AS to run normally below 45°C)

The advantage of this configuration was that the AS evaporator temperature could be raised from 16°C to a higher temperature of 20°C, with the higher corresponding vapor pressure. The resulting vapor pressure on the absorber side was then higher, meaning that a more dilute solution could be used to avoid crystallization. The other advantage is that a small VCS was required with respect to its capacity. As a result of the small

temperature lift (<10°C), a small pressure ratio (PR) (~2), a high COP (~6.4), and a fairly low compressor power was achievable. In this configuration it was found that the added parasitic power was around 800 Watts, with a resulting crystallization temperature margin of 12.7°C at the design condition. Ideally, the supplemental VCS should not be run at all conditions since it would be an unnecessary parasitic power in most cases. A simple control strategy would involve placing a bypass line in the evaporator water loop to allow it to go directly to the air to be cooled. This would enable the supplemental VCS to be turned off at lower ambient conditions where crystallization is not an issue. The dotted line around the VCS in Figure 21 shows this bypass line.

The VCS model for the cascaded system was adapted from the VCS model used for the legacy system. The values for the cascaded VCS are shown alongside the values used for the conventional VCS for comparison in Table 8. Differences worth noting are the isentropic efficiency, evaporator outlet temperature, and condenser inlet temperature. The isentropic efficiency was based upon the PR, as defined below in Eq. 11 [35].

$$\eta_{isentropic} = 0.85 - 0.0467 * PR \qquad\qquad (11)$$

As a result, the lower PR for the supplemental VCS resulted in a better isentropic efficiency. The evaporator air outlet for the conventional VCS was set at a typical value of 5°C to reflect its usage for cooling in usual cases as opposed to the 19°C which would allow just enough dehumidification for this set point. The condenser temperature for the supplemental VCS was lowered to match the temperature of the AS evaporator due to its position nearby, rather than being located in the outside ambient air. One of the benefits of this configuration is that the COP of this VCS was very high, due to the low condenser temperature resulting from its heat exchange with the AS evaporator.

Table 8: Key modeling assumptions for VCSs (Supplemental VCS has better isentropic efficiency due to smaller PR, lower condenser inlet temperature due to placement in the AS evaporator, 5°C outlet of conventional VCS due to lower evaporator temperature for which VCSs are typically capable)

	Conventional VCS	Supplemental VCS for cascaded
Evaporator approach temperature	7°C	7°C
Condenser approach temperature	5°C	9°C
Superheat	10°C	10°C
Subcooling	5°C	5°C
Compressor isentropic efficiency	0.61	0.8
Compressor motor efficiency	0.85	0.85
Evaporator air inlet	38.9°C	38.9°C
Evaporator air outlet (T, RH)	5°C, 100%	19°C, 100%
Condenser air/water inlet	51.7°C	22°C (water)
dP in evaporator (refrigerant)	50 kPa	50 kPa
dP in condenser (refrigerant)	100 kPa	100 kPa

The supplemental VCS was included in the EES model as a module in order to integrate its effect. However, its parasitic load was not included directly in the curve fits, but included separately later in TRNSYS. Heat exchanger diagrams for the AS and VCS evaporators at the design conditions are shown in Figures 22 and 23. The first diagram describes the first part of the water loop starting with the AS evaporator. T[9] enters the AS evaporator at a temperature of 20°C, cooling the entering water stream from a temperature of 23.3°C to 22°C. The temperature of the AS refrigerant remains the same due to the two-phase region, and the water loop ΔT is kept low due to a high flow rate in the water loop. On the other side of the water loop, the water which has just been chilled now cools the refrigerant of the VCS condenser from superheated 52°C down to a subcooled temperature of 25°C. Figure 23 shows what occurs on the other side of the VCS, at the evaporator side. The lower line shows the two-phase region with pressure drop and a 10°C superheat region. This occurs while the supply air is cooled from 39°C to 19°C.
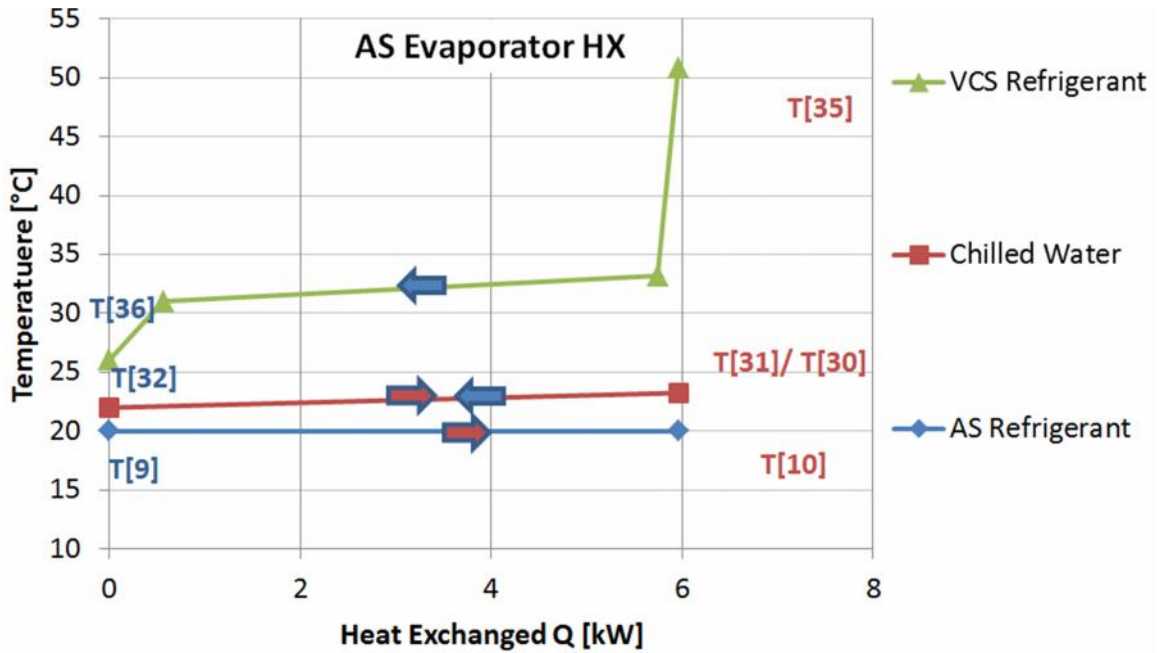
Figure 22: T-Q diagram for cascaded system (AS evaporator refrigerant, the bottom line, is heated as a two-phase mixture as the water loop, the line above it, is chilled. Considering the same T and line, the other side of the water loop then chills the VCS condenser refrigerant which is the top line)
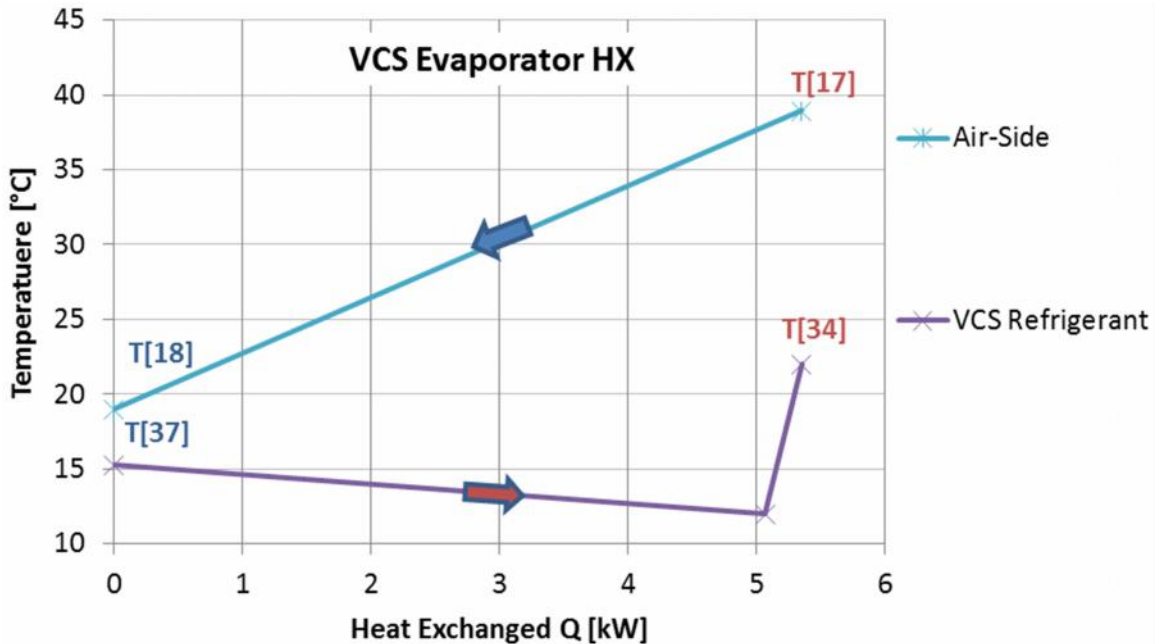
Figure 23: T-Q diagram for cascaded system (VCS evaporator refrigerant heated through two-phase region with pressure drop and 10°C superheat, as supply air is cooled from 39°C to 19°C)

Similar to the baseline AS, the individual parasitic loads were estimated and summed based upon identified manufactured products. The only additional one shown here is the pump to account for the water loop between the AS evaporator and the VCS condenser. Table 9 shows the details of the parasitics for the system. The sizes of the two Grundfos pumps were estimated based on their pictures since the actual dimensions were unavailable. The 820 W load of the supplemental VCS and the 150 W of the duct burner also contributed to the total parasitic load of this system. The supplemental VCS load was not included in the curve fit as it was to be calculated separately within TRNSYS.

Table 9: Parasitic loads of fans/pumps for cascaded AS [36]

Parasitic Loads	Manufacturer	Model	Weight [kg]	Size [m^3]	Parasitic Electricity [W]
Makeup Air Fan	Panaflo	FBA09A12V	0.40	2.15E-04	4.80
Return Fan	Suncourt	DB208	1.36	6.59E-03	82.50
Condenser Fan	Suncourt	DB210	2.04	1.03E-02	165.00
Absorber Fan	EBM Papst	W2E250	1.81	6.25E-03	175.00
Duct Burner Fan	Sanyo Denki	109P0412H602	0.40	3.52E-05	1.32
Solution Pump	Grundfos	Alpha	3.15	2.83E-02	45.00
Water Loop Pump	Grundfos	UPS26-99	4.64	2.83E-02	124.00
Desorber Fan	Theoretical Calc		0.4	2.15E-04	8.29
Sum			14.20	0.05191	605.91

The curve fits graphs related to the cascaded system are shown in Figures 24 to 28, with the corresponding equations given in the Appendix, Eqs. 52-56. The curve fit for the COP, when the duct burner was off was considered the same as the baseline model. The additional evaporator load ($Q_{evaporator}$) curve fit was necessary as it accounted for the slightly higher load on the AS evaporator due to the VCS, as opposed to using the strict $Q_{evaporator}$ calculation of Eq. 6.
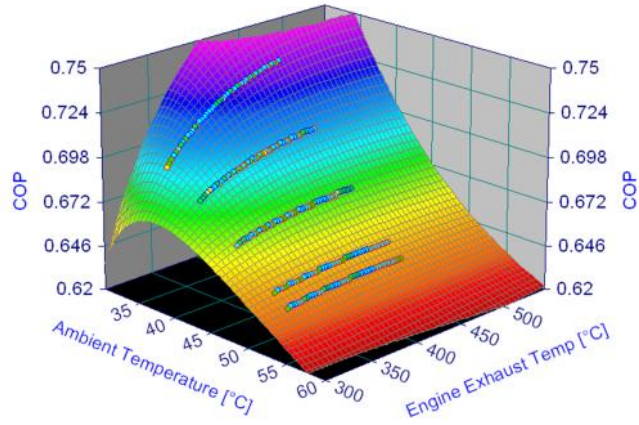
Figure 24: Cascaded AS COP curve fit for duct burner on (COP varies between 0.63 to 0.74, staying consistent due to high quality waste heat available when DB is on)
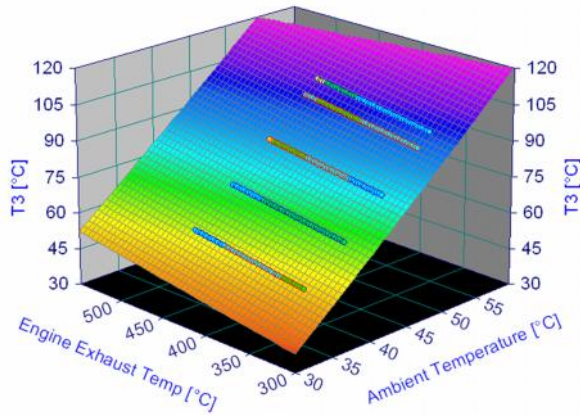
Figure 25: T₃, LiBr solution temperature entering desorber for cascaded AS (used to model the desorber HX in TRNSYS)
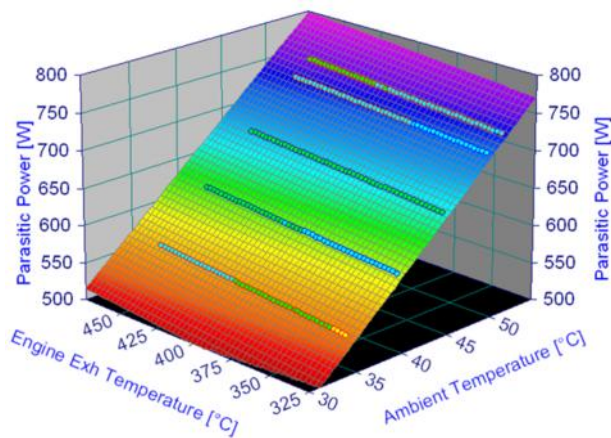
Figure 26: Cascaded AS parasitic power curve fit for duct burner on (includes DB fuel pump and extra water loop pump, but supplemental VCS parasitic is not included here)
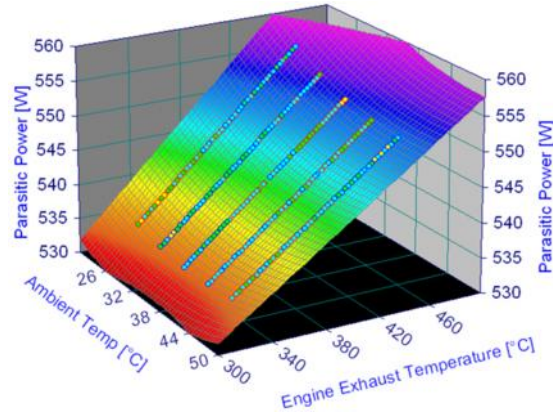
Figure 27: Cascaded AS parasitic power curve fit for duct burner off (only small variations in parasitic power, because DB fuel pump is not running, but fan power still varies slightly with flow rates)
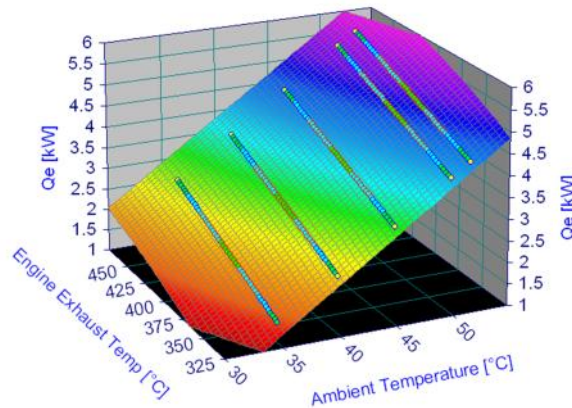
Figure 28: Cascaded AS Q_e curve fit for duct burner on (necessary curve fit due to the higher evaporator load as a result of heat exchange with the VCS condenser)

3.3 MIAE AS Model

Similar to the way that the baseline AS model was adapted to the conditions for the cascaded system, the same was done for the MIAE system. The MIAE configuration differed from the baseline in that it required water loops for the evaporator and absorber, which incorporate additional pumps for proper function of the MIAE. Figure 29 shows the basic layout of the MIAE system with the additional components compared to the baseline AS.
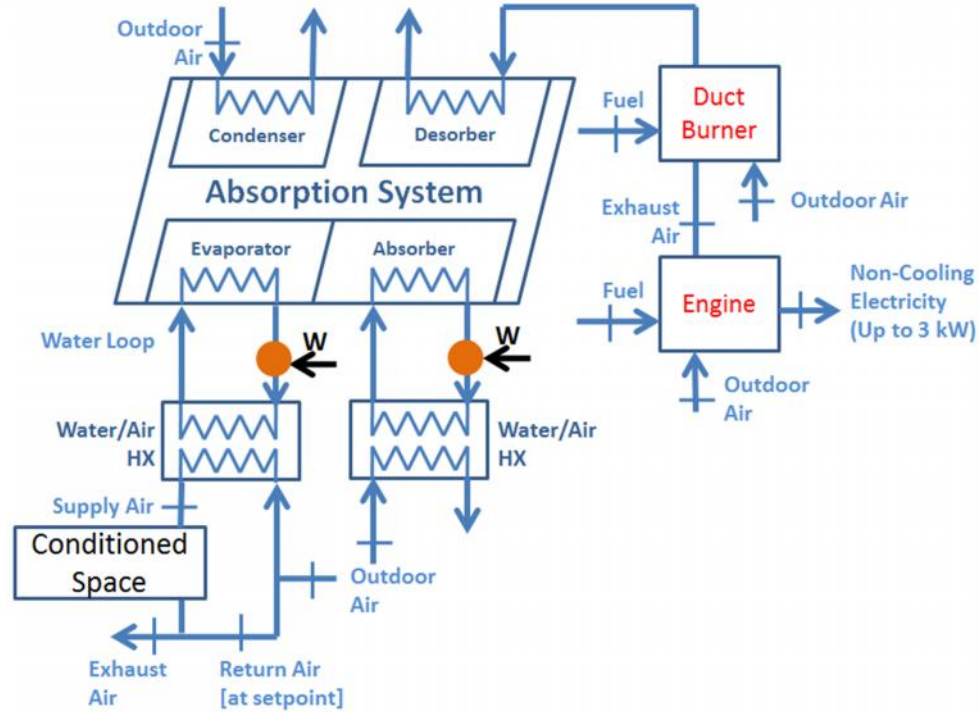
Figure 29: Overall MIAE AS schematic diagram (additional components over baseline system include the two water/air HXs and water loop pumps)

In this case, the evaporator and absorber form a single unit, but exchange heat with liquid rather than air, through the use of corresponding water loops and pumps. Additionally, this required the inclusion of two additional water/air HXs. The EES model was therefore modified to have larger UA values for the evaporator and absorber, consistent with the better heat transfer achievable with liquid over air. The EES model also included the anti-crystallization specific details as explained by the project sponsors. The parasitic loads for the pumps and fans were calculated as for the previous two AS's. In addition to the components described for the baseline AS, there were two pumps to circulate the liquid through the water loops, and two other pumps specifically applied for the MIAE system. A pump was required between the condenser and evaporator and an additional pump to recirculate water elsewhere in the AS. This brings the total AS

43

parasitic load to 847 Watts, with further details in Table 10. The pumps are all from manufacturer Grundfos, with size estimates as previously done. The curve fits derived from the EES model are displayed in Figures 30 – 34, again with the respective equations listed in the Appendix as Eqs. 57-61.

Table 10: Parasitic loads of fans/pumps for MIAE AS [36-38]

Parasitic Loads	Manufacturer	Model	Weight [kg]	Size [m^3]	Parasitic Electricity [W]
Makeup Air Fan	Panaflo	FBA09A12V	0.40	2.15E-04	4.80
Return Fan	Suncourt	DB208	1.36	6.59E-03	82.50
Condenser Fan	Suncourt	DB210	2.04	1.03E-02	165.00
Absorber Fan	EBM Papst	W2E250	1.81	6.25E-03	175.00
Duct Burner Fan	Sanyo Denki	109P0412H602	0.40	3.52E-05	1.32
Solution Pump	Grundfos	Alpha	3.15	2.83E-02	45.00
Evaporator Water Pump	Grundfos	UPS26-99	4.635	2.83E-02	124.00
Absorber Water Pump	Grundfos	UPS15-55	2.7	2.83E-02	87.00
Condenser Pump	Grundfos	UPS26-99	4.635	2.83E-02	124.00
Water Recirculator	Grundfos	UP 15-42	3.29	2.83E-02	30
Desorber Fan	Theoretical Calc		0.4	2.15E-04	8.29
Sum			24.82	0.1368	846.91
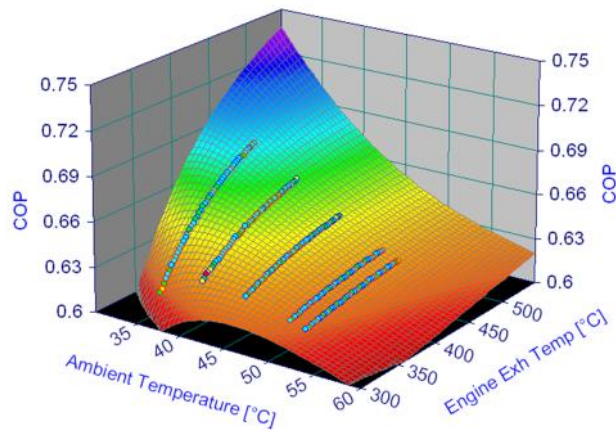
Figure 30: MIAE AS COP curve fit for duct burner on (COP is highest when the ambient temperature is low with high waste heat temperature, and lower with higher ambient temperatures)
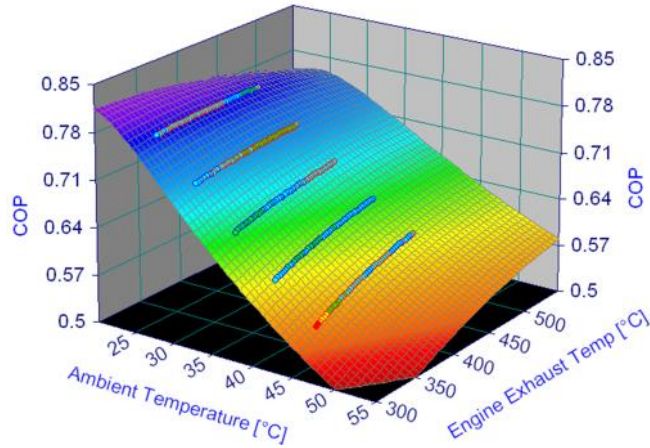
Figure 31: MIAE AS COP curve fit for duct burner off (COP is highest with the lower ambient temperature and highest engine exhaust temperature, and lowest with the higher ambient temperatures)
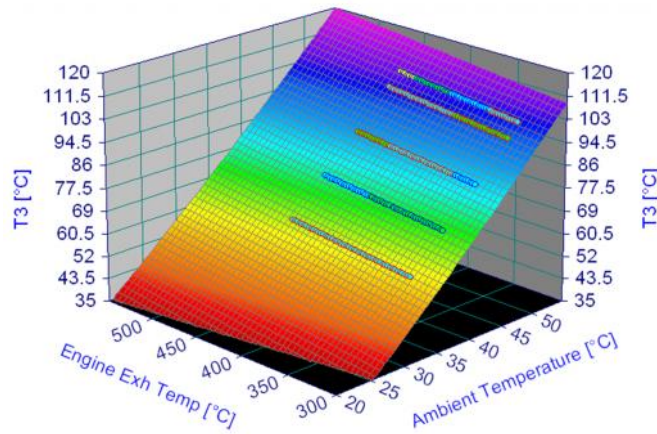
Figure 32: T₃, LiBr solution temperature entering desorber for MIAE AS (used to represent the desorber HX in the TRNSYS model)
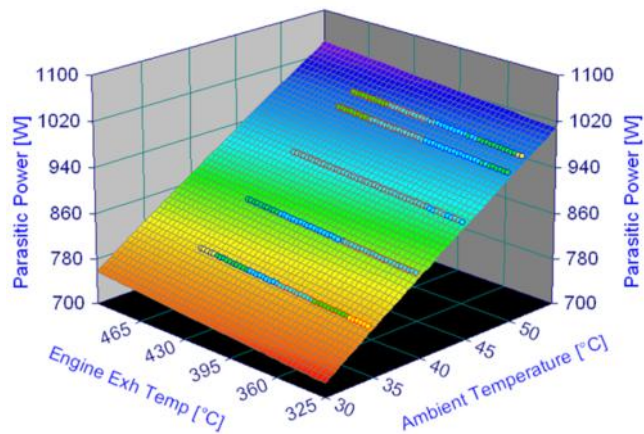
Figure 33: MIAE AS parasitic power curve fit for duct burner on (has the highest parasitic load due to many pumps, as high as around 1 kW, and varies with ambient temperature as the flow rates and DB fuel pump load decreases)
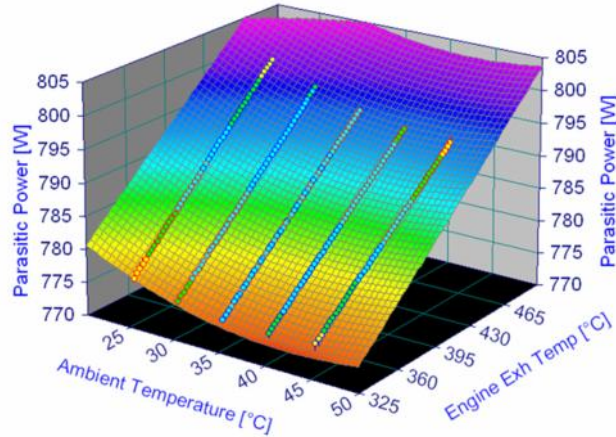
Figure 34: MIAE AS parasitic power curve fit for duct burner off (small change in parasitic loads due to small changes in fan speed and power)

3.4 Overall Modeling Approach

For an overall view of the different system models, Table 11 shows relevant values for the VCS, AS, and Gensets for each system at the design point.

Table 11: Details of each system model

System Configuration	AS Cooling Capacity [kW]	VCS Cooling Capacity [kW]	AS COP	VCS COP	Parasitic Power [kW]	VCS Compressor Power [kW]	Genset Size [kW]
Legacy	N/A	5.275	N/A	1.06	N/A	5	10
Baseline AS	5.275	N/A	0.621	N/A	0.632	N/A	5
Cascaded AS	6	5.275	0.644	6.44	1.575	0.819	5
MIAE AS	5.275	N/A	0.627	N/A	0.997	N/A	5

Table 12 displays the values relevant to the HX of each AS. Some of the notable differences amongst them are the different evaporator and absorber heat exchanger types, particularly in the cascaded and MIAE configurations. This was due to the water loops. The effectiveness for the cascaded AS evaporator was low in particular because of the approach temperatures that were set in order to maintain a conservative estimate. This resulted in a minimum ΔT of 2°C as seen previously in Figure 22 in order to be overly

46

conservative. In actuality, a counter flow water-to-water heat exchanger may be able to get closer. The effectiveness was higher for the MIAE evaporator and absorber heat exchangers due to the parallel configuration, which had particularly low mass flow rates leading to good heat exchange. The parallel configuration was unique to the MIAE because of the way that heat and mass transfer occurs, which also allowed for a close match between temperature changes on the solution side and liquid side. Consequently, this meant a higher HX effectiveness since this metric is based upon temperature differences. The desorber UA value for the MIAE was able to be increased slightly by comparison to the baseline model, up to 0.022 from 0.02 kW/K. This was because it would operate at a higher engine output for all cases as compared with the baseline system due to the additional pumps for the water loops. The result is that at the lowest operating condition and ambient temperature, the temperature leaving the desorber can be made to match that of the baseline with a higher UA value and still avoid the acid dew point limitation. Accordingly, it meant that slightly more of the exhaust heat in the MIAE system would be usable.

Table 12: Details of AS heat exchangers (lower cascaded HX effectiveness due to set approach temperatures, higher for MIAE due to unique parallel flow for heat and mass transfer, higher UA for MIAE desorber due to higher operating engine part load, UA values set higher for other HXs due to heat exchange with refrigerant instead of air)

AS model	AS HX	Absorber	Desorber	Condenser	Evaporator	Solution HX
Baseline	Type	solution-to-air	exhaust gas-to-solution	water-to-air	water-to-air	solution-to-solution
	UA Value [kW/K]	0.9	0.02	0.6	0.42	0.074
	HX_eff @ design Point	69%	71%	85%	80%	64%
Cascaded	Type	solution-to-air	exhaust gas-to-solution	water-to-air	water-to-water	solution-to-solution
	UA Value [kW/K]	0.9	0.02	0.6	2.25	0.074
	HX_eff @ design Point	69%	73%	85%	39%	64%
MIAE	Type	parallel flow, solution-to-water	exhaust gas-to-solution	water-to-air	parallel flow, water-to-water	solution-to-solution
	UA Value [kW/K]	1.8	0.022	0.6	2.25	0.074
	HX_eff @ design Point	84%	72%	85%	96%	64%

Figure 35 shows on a D hring plot the typical path of the solution as it enters and passes through the absorber for the baseline, cascaded, and MIAE AS's. It can be seen that the baseline AS in red passes the green crystallization line, whereas both the MIAE and the cascaded AS stay outside of the crystallization range, maintaining a reasonable margin.
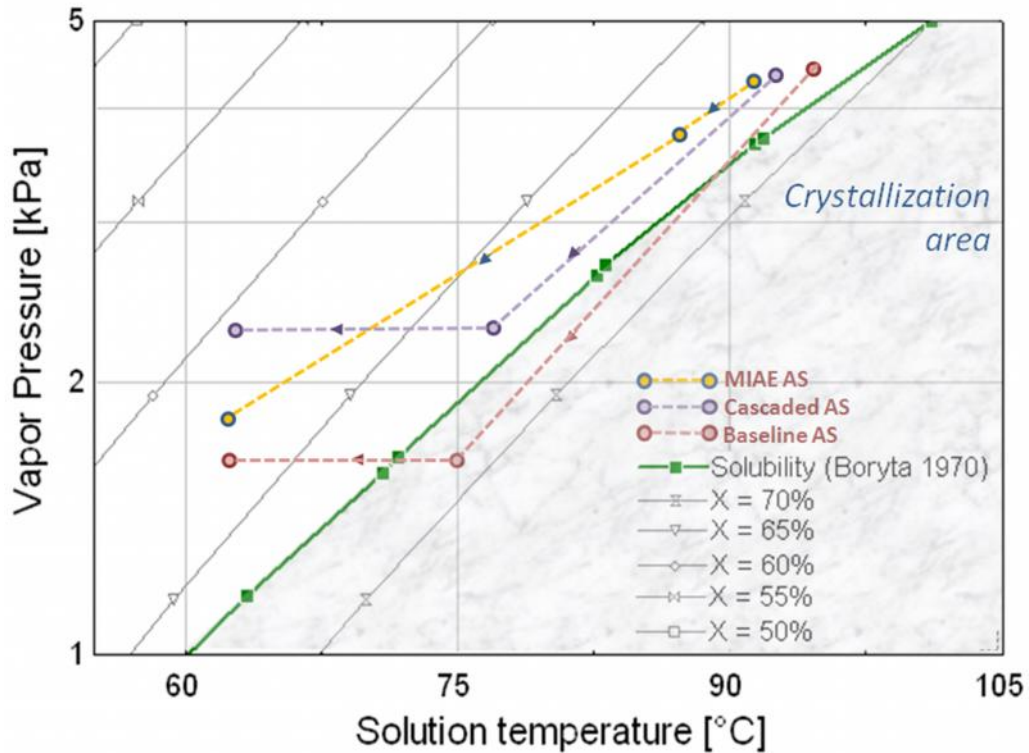
Figure 35: AS paths with crystallization at 51.7°C ambient temperature (shown is the section of concentrated solution exiting the solution HX, passing through the expansion valve, and then entering the absorber. The baseline AS clearly enters the crystallization region, while the MIAE and cascaded systems are able to avoid it)

Following the procedure shown in Section 1.1, the FCC at the design temperature was calculated for each of the cooling systems associated with each overall system. The results and procedural values are shown in Table 13. The higher the FCC efficiency, the better the usage of fuel and performance, demonstrating that the absorption systems would operate with better cooling performance at the design condition than the legacy cooling technology. This is true even for the cascaded AS which required the

supplemental VCS, but would operate with even better efficiency similar to that of the baseline AS at cooler ambient temperatures where the risk of crystallization is minimized. Therefore, in order of most efficient system operation at the design point is the baseline, MIAE, cascaded, and lastly the legacy system.

Table 13: Fuel chargeable to cooling efficiency calculation values (the AS's are shown to have much better efficiency values than the legacy VCS, with the cascaded as the lowest of the AS's due to the load of the supplemental VCS)

	Legacy	Baseline	MIAE	Cascaded
Ambient Temp [°C]	52	52	52	52
Hotel Power [kW]	3	3	3	3
$_{Elec}$ [%]	21.4%	20.9%	21.5%	21.9%
COP_{VCS}	1.06	n/a	n/a	6.44
Total Electrical [kW]	8.00	3.63	4.00	4.44
Q_{Fuel} Total [kW]	37.4	23.9	24.0	27.6
Q_{Fuel} non-cooling [kW]	14.0	14.4	13.9	13.7
FCC [kW]	23.4	9.6	10.0	13.9
FCC Efficiency	**0.225**	**0.551**	**0.525**	**0.379**

Chapter 4: Transient Simulations with TRNSYS

TRNSYS offers numerous advantages when it comes to modeling, offering the opportunity to incorporate transient profiles, flexible components, and data output for processing. The main benefit in the context of this application was the ability to combine all of the various constituents of the system together for comparison against one another. Namely, this included the cooling system, engine, weather profile, cooling load profile, and non-cooling electrical load profile.

4.1 Legacy System

The legacy system was modeled in TRNSYS, incorporating all of the data relevant to the various components, profiles, and unit/data processing. The TRNSYS diagram is shown in Figure 36 in order to display the components that were incorporated in the model. Following the load profile for the NC electrical load shown previously in Figure 2, Type 14h was used to incorporate this information into the TRNSYS model. For the weather profile, Type 109 was used to import the Meteonorm weather data for the specified location and time, namely Abu Dhabi of the United Arab Emirates for approximately week 32 of the year (5,410 to 5,578 hours) for the hottest transient weather profile.
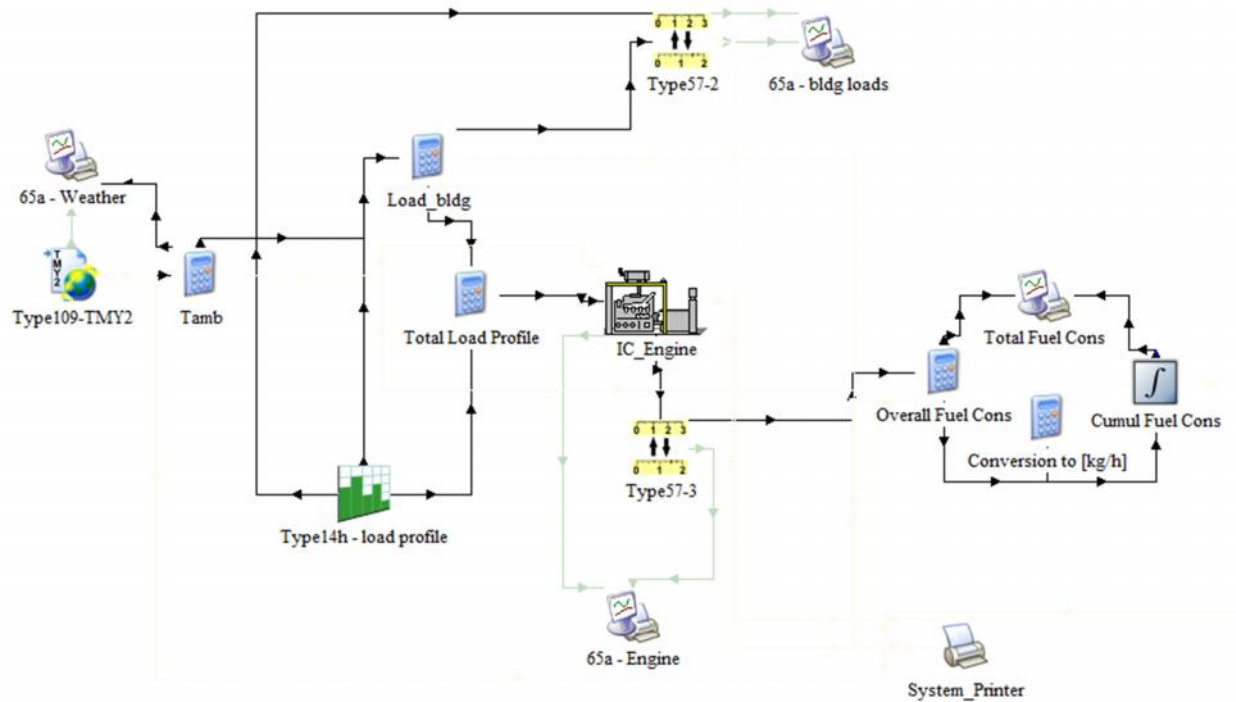
Figure 36: TRNSYS schematic of legacy system (main components include the weather components on the left, passing temperature to the calculation of the building cooling load and VCS COP; total load profile combines the electrical load of the VCS and the NC electrical load; inputs to the engine include the ambient temperature and total electrical load, outputting the fuel consumption rate and then summing the fuel usage)

The building load used the equation for cooling load as shown in Eq. 6, and was input using the equation feature of TRNSYS which appears as a calculator graphic. The total load profile calculation combined the NC electrical profile with the electrical load for cooling. The latter was calculated using the cooling load in conjunction with the VCS COP curve fit which determined the required electrical input.

The engine chosen was an internal combustion (IC) engine, Type 907, and its dat file was modified to match the expected fuel consumption and performance of the engine in Table 1. This was sized for the 10 kW legacy Genset. For the absorption based models, its capacity was then scaled down in the engine component to the 5 kW maximum output

51

size, so as to use the same engine criteria for each model. The flow rate of engine exhaust was also adjusted for scaling the engine size, as described later.

Various assumptions were used for the creation of the engine model, including the experimental data on the 3 kW engine. The engine specs were rated at an ambient temperature of 35°C. A constant specific heat, C_p, for the engine exhaust was used in both the EES and TRNSYS models, specified as 1.2 kJ/Kg K. Since the 3 kW Genset was based upon the Yanmar L70 engine [10], many of the engine calculations were based upon this engine's specifications. This included the fixed engine speed at 3600 RPM, with a displacement of 320 cc/revolution for the single cylinder, air-cooled, 4 cycle engine. The engine volumetric efficiency was 85%. A constant air density of 1.075 kg/m^3 was used below 35°C. Density of the diesel fuel was 832 kg/L, with a lower heating value of 43 MJ/kg. De-rating specifications for this engine were not found and so were based on similar specs for a Lister Petter engine [39]. The engine power and mass flow rate de-rate by 0.5% for every 1°C above 35°C, which results in 87.5% of capacity at 60°C. The input of rated exhaust flow rate for the TRNSYS engine component was scaled linearly with the rated engine capacity from the calculated exhaust flow rate. The flow rate of the engine exhaust was calculated for the 3 kW sized engine as the intake plus the fuel consumption, as per Eq. 14. This resulted in an exhaust flow rate of 0.00908 kg/s for the 3 kW engine, which when scaled linearly for the 10 kW engine yielded an exhaust flow rate of 0.03027 kg/s. The intake volumetric flow rate was calculated as shown in Eq. 12, with the factor "0.5" introduced to account for the 4 cycle characteristic. This is because every other rotation pulls air into the cylinder instead of every rotation. The input variables to TRNSYS include $_{mech}$, $_{elec}$, and f_{exh}, their derivations and

equations are listed below in Eqs. 12 through 23. These symbols respectively represent the mechanical efficiency (net work output efficiency before generator), electrical efficiency (includes generator efficiency), and fraction of energy input available in the exhaust. $_{elec}$, $_{mech}$, and f_{exh}, are not direct functions of ambient temperature, but of engine power, and so are indirectly de-rated by the higher ambient temperatures. These values were interpolated based on the power output, and lie between their values for 75% and 100% part load for the higher temperatures.

$$Volumetric\ Flow\ Rate\ (VFR)\ Intake\ [m^3/s] =$$

$$\eta_{volumetric} * Engine\ Displacement * 0.5 * Engine\ Speed \qquad (12)$$

$$Mass\ Flow\ Rate(MFR)\ Intake[kg/s] = VFR\ Intake * \rho_{air} \qquad (13)$$

$$MFR\ Exhaust\ [kg/s] = MFR\ Exhaust + Fuel\ Consumption \qquad (14)$$

$$Air\ Fuel\ Rato(AFR) = \frac{MFR\ Intake}{Fuel\ Consumption} \qquad (15)$$

$$Q_{fuel}[kW] = LHV * Fuel\ Consumption \qquad (16)$$

$$\eta_{elec} = \frac{P_{elec}}{Q_{fuel}} \qquad (17)$$

$$\eta_{mech} = \frac{\eta_{elec}}{\eta_{Generator}} \qquad (18)$$

$$P_{shaft}[kW] = \eta_{mech} * Q_{fuel} \qquad (19)$$

$$f_{exhflow} = \frac{MFR_{exhaust}}{MFR_{exhaust}@\ Full\ PL} \qquad (20)$$

$$Q_{WH}[kW] = Q_{fuel} - P_{shaft} \qquad (21)$$

$$Q_{exh}[kW] = f_{exh} * Q_{WH} \qquad (22)$$

$$T_{exhaust}\ [°C] = \Delta T + T_{ambient} \qquad (23)$$

The above equations were used to determine the inputs for the component. Subsequently, the method pursued to provide the necessary verification of the engine component was to manually calculate the engine exhaust temperature using these inputs and then compare them to the outputs from TRNSYS. This required a derivation of the temperature change starting with an energy balance for the engine. The derivation steps are shown below in Eqs. 24 through 34.

$$Q_{Exh} = c_p * m_{exh} * \Delta T \tag{24}$$

$$Q_{Exh} = f_{exh} * Q_{Waste\ Heat} \tag{25}$$

$$Q_{Exh} = f_{exh} * (Q_{fuel} - P_{Shaft}) \tag{26}$$

$$\Delta T = \frac{f_{exh} * (Q_{fuel} - P_{Shaft})}{m_{exh} * C_p} \tag{27}$$

$$P_{shaft} = Q_{fuel} * \eta_{mech} \tag{28}$$

$$\Delta T = \frac{f_{exh} * Q_{fuel} * (1 - \eta_{mech})}{m_{exh} * C_p} \tag{29}$$

$$Q_{fuel} = \frac{P_{elec}}{\eta_{elec}} \tag{30}$$

$$m_{exh} = f_{exh} * MFR_{exh} \tag{31}$$

$$P_{elec} = PLR * Rated\ Size \tag{32}$$

$$\Delta T = \frac{(f_{exh} * PLR * Rated\ Size)}{m_{exh} * C_p * \eta_{elec}} * (1 - \eta_{mech}) \tag{33}$$

$$T_{Engine\ Exhaust} = \frac{(f_{exh} * PLR * Rated\ Size)}{m_{exh} * C_p * \eta_{elec}} * (1 - \eta_{mech}) + T_{ambient} \tag{34}$$

Eq. 34 shown above was used to create the graph in Figure 37 of the engine exhaust temperature as a function of the ambient temperature at different engine part loads. The reason for the change in slope above the 35°C rated temperature, is due to the change in air density at higher temperatures as a part of de-rating for the engine. As a result, m_{exh}

in the denominator of Eq. 34 is smaller, making the term larger, and consequently effecting a larger ∆T. Figure 37 is the same whether calculated using Eq. 34 alone or plotted with output values from TRNSYS, thus demonstrating the consistency of the engine component.
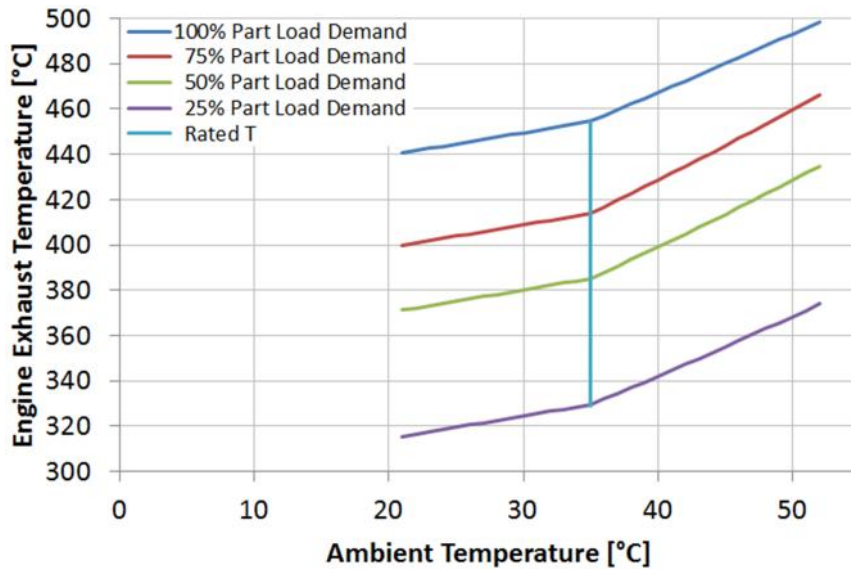
Figure 37: Diagram demonstrating the ∆T through the engine component (change in slope is due to change in air density at higher temperatures for engine de-rating; graph is the same either when plotted from TRNSYS outputs or from governing equations)

4.2 AS TRNSYS Model Components

Primarily, the TRNSYS models consisted of either built-in components or modified components. The exception to this, of course, was the AS for each case included curve fits of COP, parasitic power, and temperature profiles. The TRNSYS model contained many more components and connections than that of the legacy system. Therefore, in order to understand how the TRNSYS system ran, a flow diagram is laid out in Figure 38 with the various components. Ellipses represent beginning and end points, diamonds represent decision points, rectangles are processes which occur, and the parallelograms represent the different profile inputs to the system. Items in green are the EES curve fits

and items in blue are regular TRNSYS components. The dotted lines outline the physical pathway of the airstream starting with ambient air entering the engine where it becomes hot exhaust, passing through the duct burner where it could be heated further, and finally moves through the AS desorber where the heat is ultimately utilized.
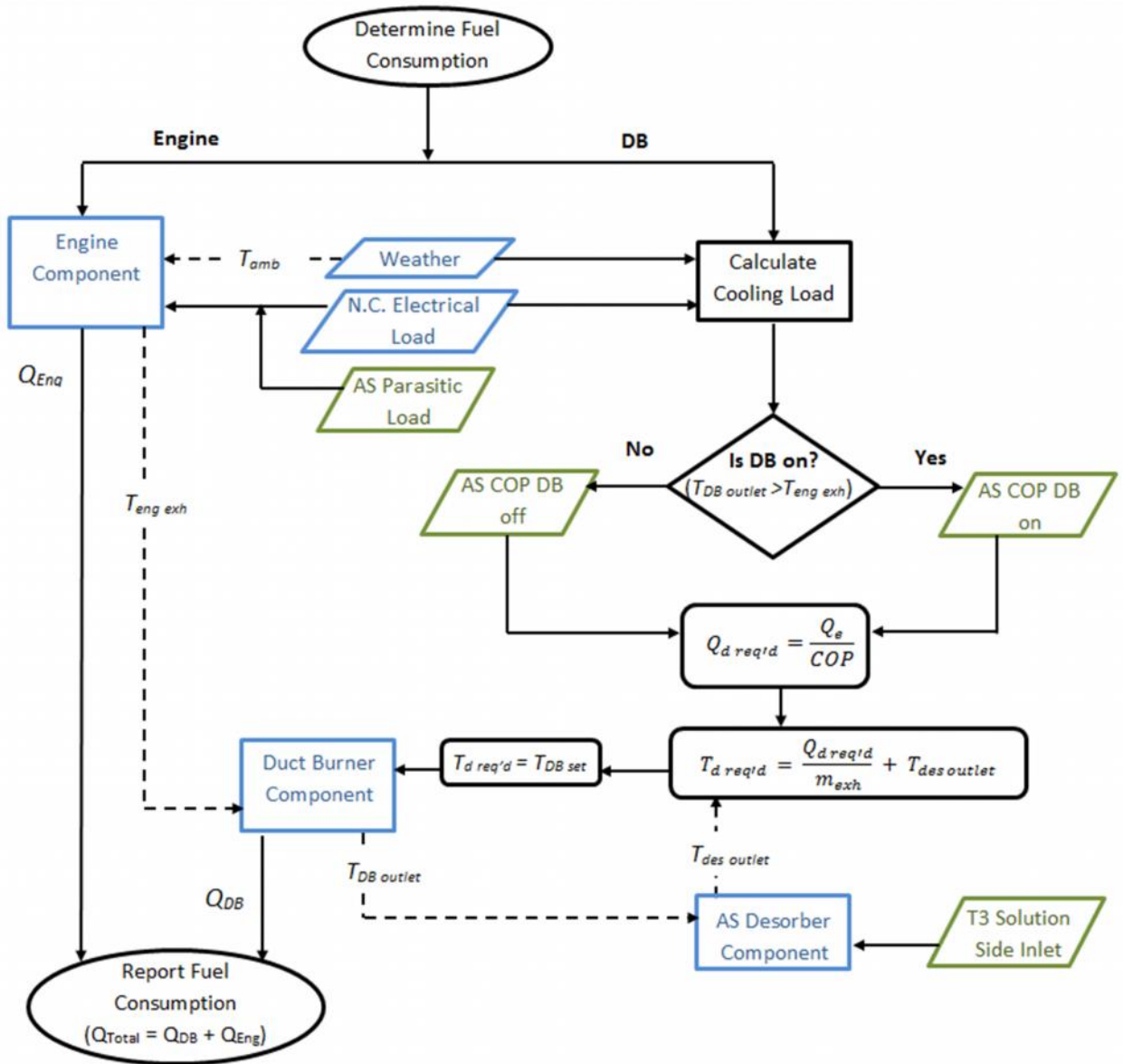
Figure 38: AS TRNSYS Flow Diagram (Ellipses represent beginning and end, diamonds represent decision points, dotted line represents physical pathway of air stream, parallelograms are profile inputs, green are EES curve fits, blue are regular TRNSYS components)

The ambient temperature and engine exhaust temperature still remained the two main independent variables as they were for the EES models. The engine exhaust temperature was taken from the engine component and the ambient temperature from the weather profile. From this model, the fuel consumption was calculated as the summation of fuel used for the engine and duct burner. On the duct burner side, the cooling load was first calculated based on Eq. 6, and then the COP was determined depending on whether the DB was on or off by comparing the DB outlet temperature with the engine exhaust temperature. Then, the required heat input for the desorber was calculated, followed by determining the required desorber inlet temperature based upon this heat load and the temperature output by the AS desorber. Depending on this DB set temperature, fuel would be burned to raise the temperature of the engine exhaust stream to the desired level. The engine fuel consumption was output by the TRNSYS engine component depending on the incoming ambient air stream and the required electrical load which was a combination of the NC electrical load and parasitic power for the AS.

As can be seen, the desorber of the AS was modeled in TRNSYS for the duct burner to function properly and to calculate temperatures for energy balances. In order to accomplish the latter, two separate models were created, each with a different desorber unit represented by Type 5b, counter flow HXs. The only difference between them was the hot air stream inlet; the lower temperature desorber had its hot side inlet temperature coming directly from the engine exhaust, where the higher temperature desorber took its hot side inlet as the duct burner outlet. The low temperature desorber was used to approximate the heat which the desorber could process from the engine exhaust gas stream alone. This proved useful in performing energy balances as discussed in Section

4.5. The higher temperature desorber was used in calculating the required temperature which in turn determined the duct burner temperature and load. The inputs for the desorber units included the Cp of the hot side as 1.2 kJ/kgK, Cp of cold side as 4.19 kJ/kgK, cold side flow rate of 108 kg/hr, heat transfer coefficient of 0.02 kJ/sK, and cold side temperature inlet from a T_3 curve fit from the EES model. These values correspond to those found in the EES model.

The weather data, load profile, engine, and fuel consumption modules were all the same as previously discussed in the legacy section. The engine component was also the same, but with a specified maximum power output of 5 kW and corresponding exhaust air flow rate of 0.015133 kg/s instead of the 10 kW, 0.03026 kg/s for the legacy system configuration. In order to get a better overall picture of how the engine model was functioning, it was useful to create an energy balance graph to display the energy distribution as a percentage of fuel input. Figure 39 shows this information for a temperature of 35°C.

This is useful to see how much waste heat is radiated and exhausted. It is also indicative of how much heat is able to be extracted through the desorber, and the amount which would be left behind. The radiation component is actually quite considerable, naturally creating the desire to capture this energy. Unfortunately, it would be difficult to retrofit an engine to recover this heat at a temperature that would be usable in the desorber. However, it does still indicate a potential avenue for investigation if desired.
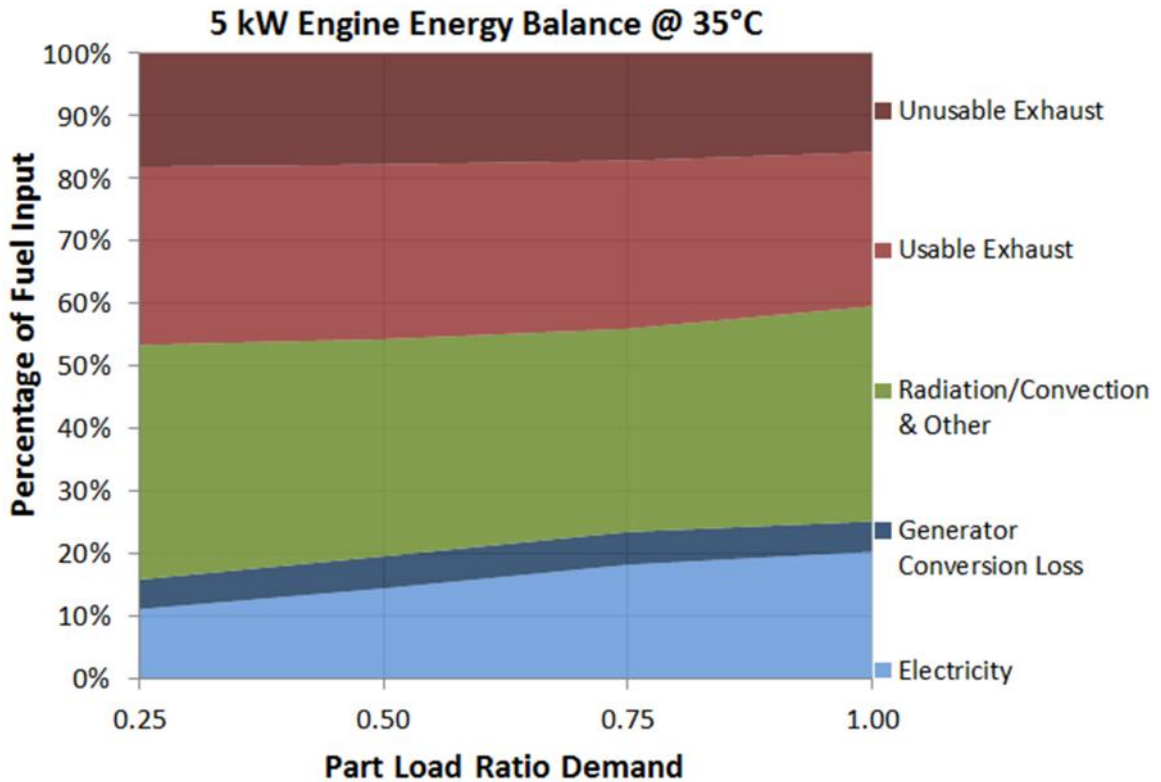
Figure 39: Energy balance of TRNSYS 5 kW engine component (the electrical efficiency is as high as about 20%, with a large portion due to radiation/convection. About 22% of the total energy input can be recovered by the AS through the exhaust air stream)

The figure also shows how the percentages of each constituent vary with the part load demand. At full load, because the engine is more efficient, a greater percentage of the fuel input is actually converted to electrical power, and the heat available in the exhaust actually decreases. It is interesting to see just how small a percentage the electrical production is, in relation to the total fuel input. This forms a small percentage only as high as 20%, which further supports the rationale for CHP utilizing a waste heat driven technology.

For the full year duration, the AS's and their parasitic loads were turned off at temperatures below 20°C. This was chosen because the humidity ratio for 20°C and 100% relative humidity matches the indoor set point of 15.2 g/kg. This means that the

indoor set point would be reached even with the cooling turned off at 20°C and below. The curve fits were included in equation units as was done for the building load. Additionally, there were a number of Type 57 units used for converting between units, Type 65a printers for visually showing the outputs, and additionally the system printer, Type 25a, which exported the raw data for external manipulation.

Determining whether the duct burner was on or off was achieved by comparing the temperature exiting the duct burner with the temperature exiting the engine. If the temperature leaving the duct burner was greater, then the system reported that the DB was on, and the correct curve fit was chosen for COP and parasitic load. The DB component was Type 659, with inputs of fluid specific heat as 1.2 kJ/kgK and rated capacity of 10 kW. The other values were defined by outputs of the other components.

The additional absorption based systems were modified starting with this AS model. The change was adapted by changing the curve fits from those pertaining to the baseline AS, to those of the cascaded or MIAE AS. The cascaded AS model required one additional curve fit, which was the AS evaporator cooling load, because this value was slightly higher than the standard one due to the supplemental VCS. Therefore, this additional curve fit was incorporated into the TRNSYS model only for temperatures above 45°C, where the VCS would be on, and the standard equation for evaporator load was used at all other temperature conditions. Additionally, the supplemental VCS load was calculated in TRNSYS separately from the parasitic load curve fit. Using the cooling load and a static COP of 6.44, the required compressor power input was calculated and reported as part of the electrical output demand. This value of COP was held constant during its operation, as its operating conditions were not dependent upon the ambient

temperature since the VCS condenser was linked to the AS evaporator instead of the outdoor air. The AS evaporator temperature was held constant when working in conjunction with the supplemental VCS, effecting a constant COP value for its operation.

4.3 Model Verifications

For a good consistency in processing the data for each system, an Excel spreadsheet template was created to interpret the results output from the printer module of TRNSYS. The data was pasted into a sheet, with units native to TRNSYS, and in another sheet the data was converted to units pertinent to the project. A useful aspect of this format was that energy balances could also be incorporated into the spreadsheet to ensure that everything made sense physically. These checks included an energy balance on the engine, the desorber, duct burner, and total heat balance, as detailed in Eqs. 35 through 39. Eqs. 35, 36, and 39 should each result in a 0% deviation between the left and right sides of the equation, ± 0.2% to allow for any rounding and difference in significant figures. When they did not fall within this range, it indicated an issue with the TRNSYS simulation or configuration. Eqs. 37 and 38 should always report positive values, indicating that the actual desorber heat was greater than the required value, thus ensuring a realistic heat input to the AS. These checks helped to troubleshoot the models when they were found to have inconsistencies. $Q_{environmental}$ is representative of the radiative heat of the engine. Q_{input} is the energy, or fuel input to the engine. $Q_{desorber\ exhaust}$ is the amount of heat in the exhaust stream that is extractable by the AS desorber. The generator conversion loss is accounted for by the shaft power lost.

$$Q_{input} = Shaft\ Power\ Lost + Electrical\ Power + Q_{engine\ exhaust} + Q_{Environmental} \qquad (35)$$

61

$$Q_{desorber} = Cp * m_{exhaust} * (T_{DuctBurner\,Out} - T_{desorber\,Hot\,Outlet})\qquad(36)$$

$$Q_{desorber} - Q_{desorber\,Required} >= 0\qquad(37)$$

$$Q_{DB\,input} + Q_{desorber\,exh} - Q_{desorber\,Required} >= 0\qquad(38)$$

$$Q_{DB\,input} = m_{exhaust} * Cp * (T_{DB\,out} - T_{Engine\,Exhaust})\qquad(39)$$

Once the components and curve fits were assembled in TRNSYS, the outputs were verified to ensure reasonable results. The verification approach for each system followed generally the same procedure. This included inspecting the outputs for values matching those from EES and the curve fits. Also carried out was a verification process by means of a rough estimation calculation. The verification involved running the model at 51.7°C ambient temperature while providing 3 kW of NC electrical power. The rough estimation procedure is detailed in Eqs. 40 through 45. The details of verification for each of the models are shown in Table 14, which correspond to the variables shown in the equations below. The verification showed that the rough calculation deviated by no more than 3.5% from the TRNSYS calculation. This difference could be attributed in part to the estimation character of the equations. They are not representative of all aspects of each component in the system, but merely a way of approximating. For example, Eq. 43 solves for duct burner input (Q_{DB}) by means of the HX effectiveness, when in actuality the desorber component incorporates more inputs and calculations. However, overall the equations follow a logical sequence, and the close match to the actual TRNSYS outputs provides a simple verification of the models.

Table 14: TRNSYS model verification values

	Legacy	Baseline	MIAE	Cascaded
Ambient Temp [°C]	52	52	52	52
Hotel Power [kW]	3	3	3	3
LHV Fuel [MJ/kg]	43	43	43	43
Duration [hrs]	168	168	168	168
η_{elec} [%]	21.4	20.9	21.5	21.9
COP_{VCS}	1.06	n/a	n/a	6.44
COP_{AS}	n/a	0.621	0.627	0.644
Desorber Effectiveness	n/a	0.682	0.718	0.679
Energy in Exhaust [%]	n/a	39.4	37.9	36.6
Total Electricity [kW]	8	3.63	4	4.44
Engine Q Input [kW]	37.2	17.3	18.6	20.3
Q_d [kW]	n/a	8.49	8.41	9.34
Q_{exh} [kW]	n/a	6.82	7.04	7.42
Q_{DB} [kW]	n/a	5.63	4.68	6.34
Total Fuel Rate [kW]	37.2	22.96	23.28	26.59
Rough Calc Fuel Consumption [kg]	523.3	323	326.9	373.9
TRNSYS Fuel Consumption [kg]	519.7	333.8	336.9	387
% Difference	**0.70%**	**3.23%**	**2.90%**	**3.36%**

$$Engine\ Q\ input = \frac{Electrical\ Load}{\eta} \tag{40}$$

$$COP = \frac{Q_{evaporator}}{Q_{desorber}}; COP\ \&\ Qe\ known;\ Gives\ Q_{desorber} \tag{41}$$

$$Q_{exhaust} = Engine\ Q\ Input * Energy\ in\ Exhaust \tag{42}$$

$$Q_{desorber} = Des_{eff} * (Q_{exh} + Q_{DB});\ des_{eff}\ known;\ gives\ Q_{DB} \tag{43}$$

$$Total\ fuel\ rate\ (Q_{total}) = Engine\ Q\ input + Q_{DB} \tag{44}$$

$$Fuel\ consumption\ [kg] = \frac{Q_{total}[kW]*time[s]}{LHV_{fuel}[\frac{kJ}{kg}]} \tag{45}$$

Chapter 5: Results of Investigated Systems

5.1 Legacy System

In addition to solving for the fuel consumption of each system, another task was to identify the weights of each system. This included estimating component weights of each system based on existing manufactured items. Details of the legacy system with the weights and volumes are shown in Table 15. The main components are the engine, the 6 kW VCS, and a one week supply of fuel for the engine. The total weight comes in at 1027 kg, with the fuel constituting a significant 37% of the overall weight.

Table 15: Legacy system weight/volume details with worst week fuel consumption

Component	Capacity	Make/Model	Weight [kg]	Size [m³]	Comment
Engine	10 kW	DRS 10 kW Genset	509.7	1.164	Water Cooled, with battery, minus 9 gals/34 litres fuel
VCS @ 120F	6 kW	AirRover ULCR24BA	139.7	0.657	A/C unit for Army purposes, 6 kW @ 120F
Week of Engine Fuel			377.3	0.454	119.8 gallons (hottest week)
Week of Duct Burner Fuel			0.0		
Totals			**1026.7**	**2.274**	

When the TRNSYS model of the legacy system was run for a one week duration at the static design condition of 51.7°C and 3 kW of NC electrical load, it resulted in a fuel consumption of 163.2 gallons of fuel. For the transient one week weather profile shown in Figure 4, the cumulative fuel consumption was 119.8 gallons of fuel, with the transient data shown in Figure 40. The full year weather data resulted in a fuel consumption of 5581 gallons of fuel, with details shown in Figure 41.
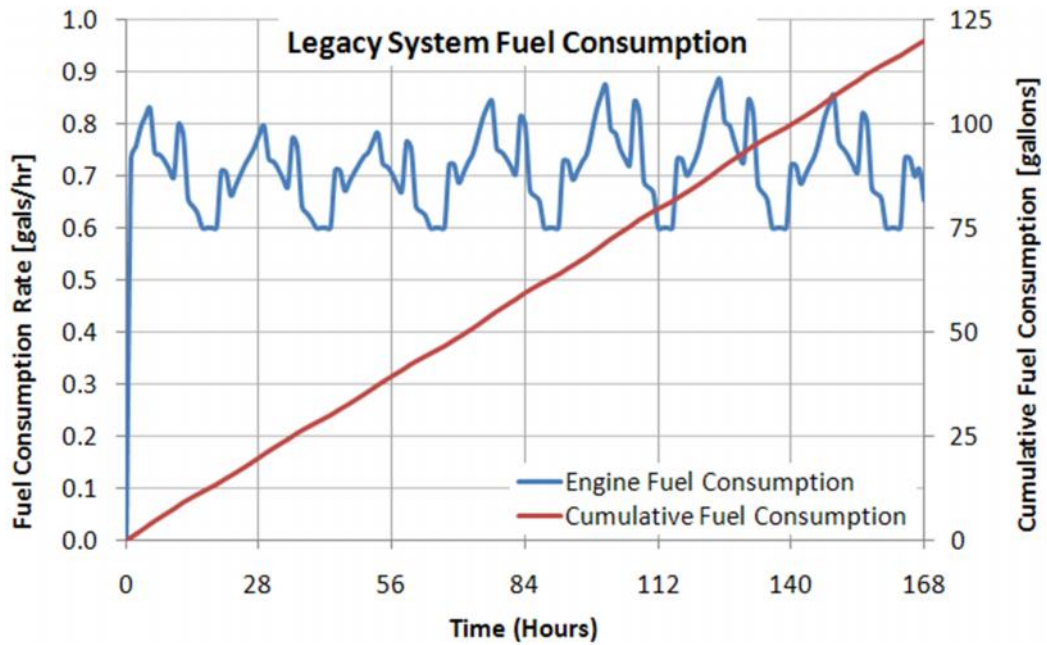
Figure 40: Legacy system fuel consumption for hottest week transient simulation (engine fuel rate varies between 0.6 and 0.9 gals/hr, with cumulative fuel for the week at just under 120 gallons)
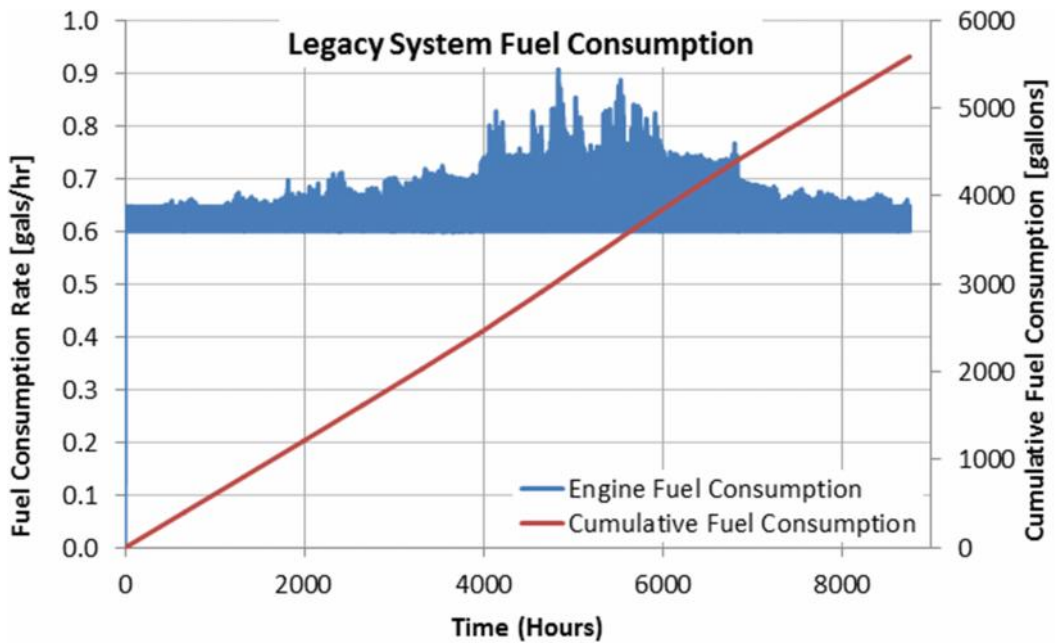
Figure 41: Legacy system fuel consumption for full year simulation duration (fuel rate is clearly highest in the summer hours, but still runs at a fairly high rate during the rest of the year, due to the large size of the Genset)

 A summary of the various baseline system constituents in terms of weight, volume, and parasitic load is shown in Table 16. This table displays the main components for the system which includes the engine, AS, duct burner, the parasitic components as discussed in Chapter 3, and the fuel for both the engine and DB. The weight and size of the AS was based upon a manufactured AS by Broad Air Conditioning [40]. The value was scaled down linearly from a 23 kW AS to the 5.275 kW capacity model relevant for this particular system. As discussed previously, a 10 kW DB from Wayne Combustion was chosen which constitutes a small portion of the total weight. The overall weight comes in at 800 kg, with a substantial 28% of the weight due to the fuel. Regarding the fuel, it is down from the 37% weight of the legacy system, with the DB consuming only 12% of the total fuel usage.

Table 16: Baseline AS weight/volume details with worst week fuel consumption [40 - 41]

Component	Capacity	Make & Model	Weight [kg]	Size [m^3]	Parasitic Electricity [Watts]	Comment
Engine	5 kW	DRS 5 kW Genset	386.9	0.959		Water-cooled, with battery, less 5 gallons fuel
Absorption System	5.275 kW	Modified Broad Air BCT23	165.9	0.573		Based on 23 kW system, 110.1 kg/ton (scaled)
Duct Burner	10 kW	Wayne Combustion MSR-DC	11.3	0.027	150.0	
Fans & Pumps	482 W	Various	9.6	0.024	481.9	
Week of Engine Fuel			199.2	0.239		
Week of Duct Burner Fuel			27.3	0.033		
Totals			800.3	1.854	631.9	

When the TRNSYS model of the baseline system was run for a one week duration at the static design condition, the result was a fuel consumption of 106 gallons of fuel, a savings

of 35% by comparison to the legacy system. Details of the transient one week simulation are shown in Figure 42, which resulted in a cumulative fuel consumption of 71.9 gallons, 40% lower than the legacy system. Finally, the full year simulation resulted in a fuel consumption of 3,217 gallons, a 42.4% savings, with graphical details shown in Figure 43. It can be seen from the graph that the duct burner is on for a significant amount of time during the hottest week as represented by the green line. In comparison to the full year profile, the DB is only on during the summer, and results in a lower base fuel consumption for the engine during the rest of the seasons.
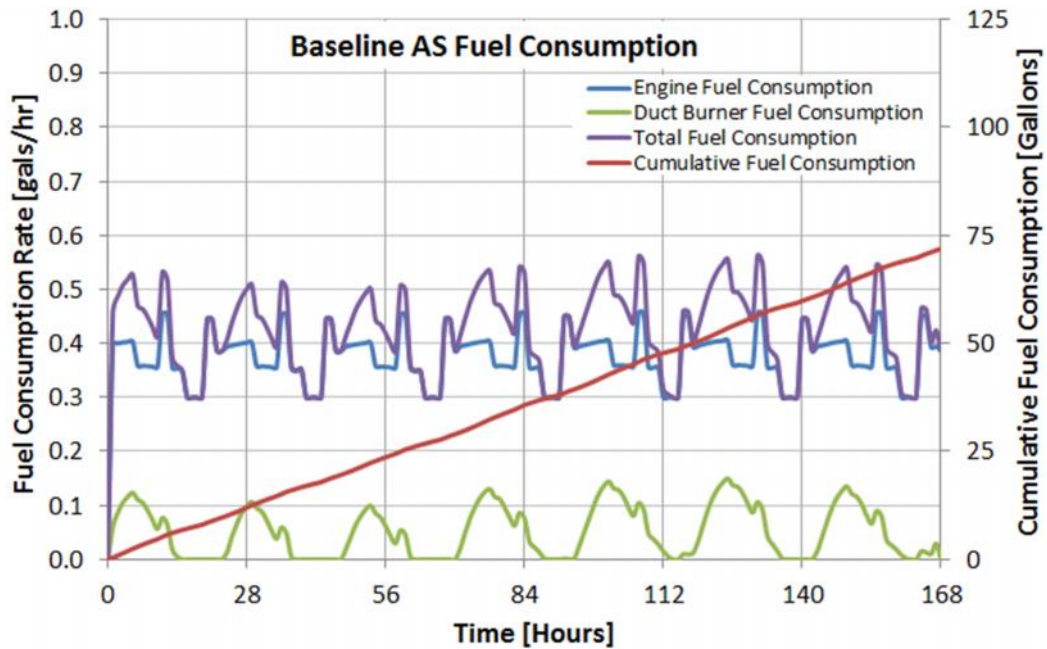
Figure 42: Baseline AS fuel consumption for transient worst week profile (total fuel consumption rate varies between 0.3 and 0.55 gals/hr, made up of duct burner and engine load, resulting in cumulative fuel of 74 gallons)
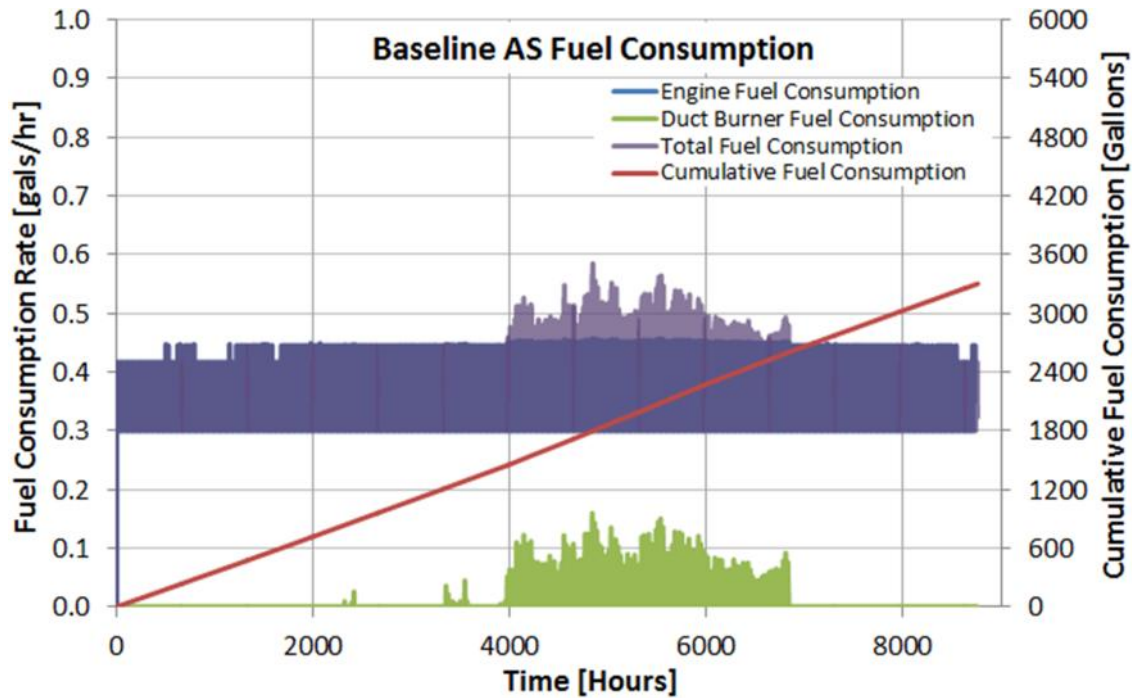
Figure 43: Baseline AS fuel consumption for transient full year profile (it can be seen that the DB runs the most during summer hours, but the system runs with a relatively low base load as low as 0.3 gals/hr)

5.3 MIAE AS

Despite the added components and parasitic loads, there was a reduction in weight and volume of the MIAE component by 30% over the conventional absorber evaporator unit. This was factored in by adjusting the weight estimation of the AS. The weights/sizes of the five main heat exchangers were estimated by scaling their respective heat loads as a fraction of the total, as shown in Table 17. Piping, unaccounted for in terms of heat load, was estimated as 10% of total size and weight, with the percentage weights of the other HXs reduced proportionally for a sum total of 100% as reflected in the table. The evaporator and absorber were then reduced by 30% and summed with the other parts to give the total weight/volume. As a result, the weight and volume of the AS were reduced from 165.9 kg and 0.573 m^3 to 146.1 kg and 0.504 m^3, respectively.

Table 17: Breakdown of AS components size/weight (used to determine the reduction in total MIAE AS volume and weight, by reducing just the evaporator and absorber by 30%)

Component	Heat Transfer [kW]	Fraction of Total Size/Weight
Evaporator	5.3	16.0%
Absorber	7.8	23.8%
Condenser	5.7	17.3%
Desorber	8.3	25.2%
Solution HX	2.5	7.7%
Piping		10.0%
Total	29.6	100.0%

However, the weights of the additional water-to-air heat exchangers needed to be considered as well. Estimates were made by using a heat exchanger design software called CoilDesigner [42]. Using the parameters specific to the MIAE model, heat exchangers were designed using a tube and louver-type fin configuration. The weights and volumes for the aluminum evaporator and absorber water-to-air HXs were 12.8 kg, 0.060 m^3, and 12.3 kg, 0.069 m^3, respectively. It is also worth mentioning that exploring a microchannel design would be a reasonable avenue to further reduce the size of these heat exchangers. In conjunction with the rest of the components, the total weight of the system was brought to 589.4 kg without considering the weight of fuel or potential savings from microchannel HXs. These details of the various components contributing to the overall system weight and volume are laid out in Table 18.

Table 18: MIAE AS weight/volume details with worst week fuel consumption

Component	Capacity	Make & Model	Weight [kg]	Size [m³]	Parasitic Electricity [Watts]	Comment
Engine	5 kW	DRS 5 kW Genset	386.9	0.959		Water-cooled, with battery, less 5 gallons fuel
MIAE Absorption System	5.275 kW	Modified Broad Air BCT23	146.1	0.505		Based on 23 kW system, 110.1 kg/ton (scaled)
Duct Burner	10 kW	Wayne Combustion MSR-DC	11.3	0.027	150.0	
Fans & Pumps	847 W	Various	24.8	0.1368	846.9	
Evaporator Water Loop HX	5.275 kW	CoilDesigner Estimate	12.8	0.060		
Absorber Water Loop HX	7.8 kW	CoilDesigner Estimate	12.3	0.069		
Week of Engine Fuel			211.8	0.255		
Week of Duct Burner Fuel			21.6	0.026		
Totals			**827.7**	**2.036**	**996.9**	

The one week design point simulation reported a fuel consumption of 107 gallons, a 34.4% savings. For the worst week transient simulation, the fuel consumption of the MIAE system was 74.1 gallons, a 38.1% savings, and details shown in Figure 44. The full year simulation showed a savings of 38.2%, with a cumulative fuel consumption of 3,450 gallons, with more detail displayed in Figure 45. As with the baseline system, the MIAE exhibits the same characteristics with the DB on continuously during the hottest week and turned off for much of the off-peak seasons.
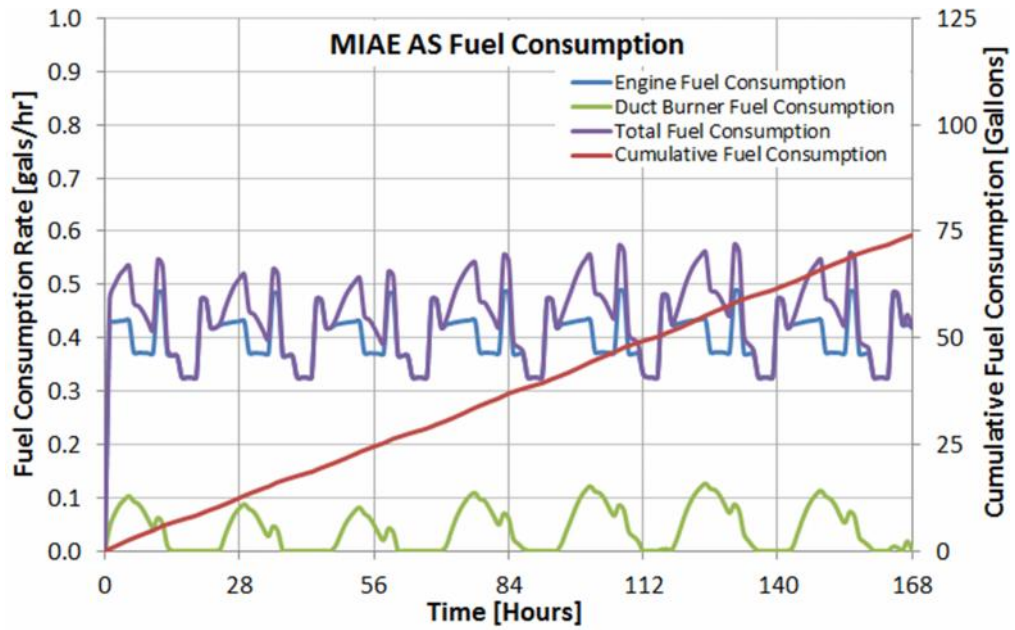
Figure 44: MIAE AS fuel consumption for transient worst week profile (just as with the baseline AS, the MIAE AS has a total fuel rate made up of the DB and engine)
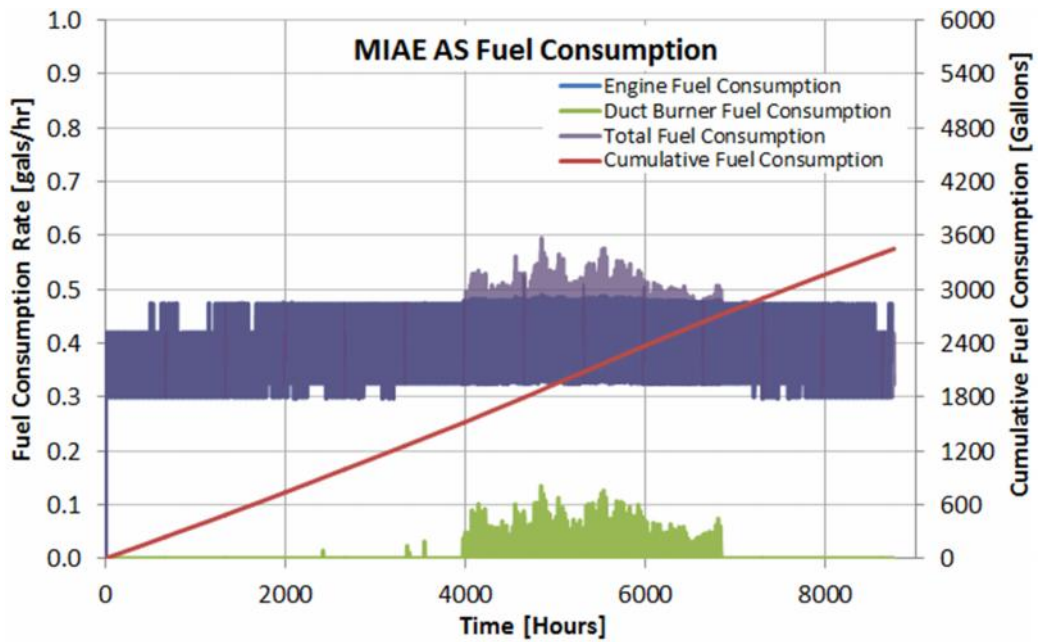
Figure 45: MIAE AS fuel consumption for transient full year profile (the DB runs primarily in the summer and runs with a slightly higher fuel rate than the baseline case)

71

5.4 Cascaded AS

In addition to the components seen in the baseline AS, the cascaded AS included an extra pump, extra HX, and also a supplemental VCS. The weight and volume of the VCS was based upon model LX-140 from manufacturer Soleus [43], scaled linearly up from the 4.1 kW rated value. The total weight of the system as seen in Table 19 was brought to 907.3 kg. The cascaded system was run for the cases of static one week design condition, worst week transient weather, and full year profile, resulting in corresponding fuel consumptions of 122.9, 71.9 and 3,217 gallons. This amounted to savings of 35%, 40%, and 42.4% respectively. Details of the worst week and full year transient simulations are displayed in Figures 46 and 47. It can be seen from the hottest week diagram that the DB was on higher than in the other systems, reaching higher peaks. This was in order to accommodate the higher AS evaporator load of 6 kW, in order to properly cool the VCS condenser.

Table 19: Cascaded AS weight/volume details with worst week fuel consumption

Component	Capacity	Make & Model	Weight [kg]	Size [m³]	Parasitic Electricity [Watts]	Comment
Engine	5 kW	DRS 5 kW Genset	386.9	0.959		Water-cooled, with battery, less 5 gallons fuel
Absorption System	6 kW	Modified Broad Air BCT23	187.2	0.573		Based on 23 kW system, 110.1 kg/ton (scaled)
Duct Burner	10 kW	Wayne Combustion MSR-DC	11.3	0.027	150.0	
Fans & Pumps	606 W	Various	14.2	0.052	605.9	
Water/Air HX	5.2 kW	CoilDesigner Estimate	12.8	0.060		
Supplemental VCS	5.27 kW	Soleus LX-140	48.0	0.230	818.7	Based on 4.1 kW system (scaled)
Week of Engine Fuel			212.0	0.255		
Week of Duct Burner Fuel			34.9	0.042		
Totals			**907.3**	**2.197**	**1,574.6**	
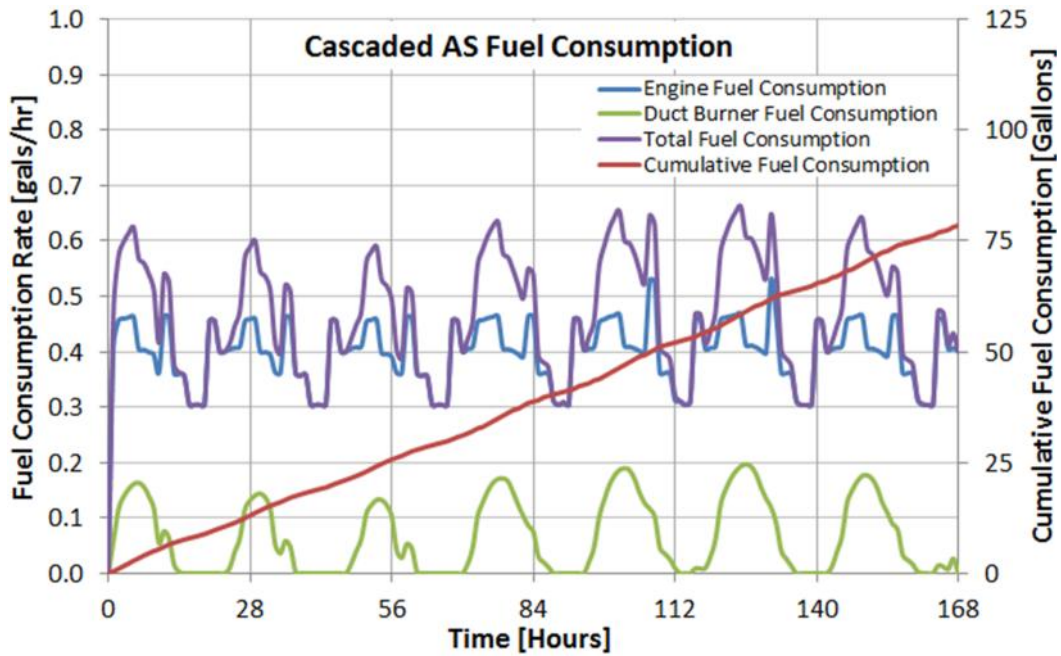
Figure 46: Cascaded AS fuel consumption for transient worst week profile (has higher peaks due to a greater electricity requirement of the greater parasitic loads of the supplemental VCS)
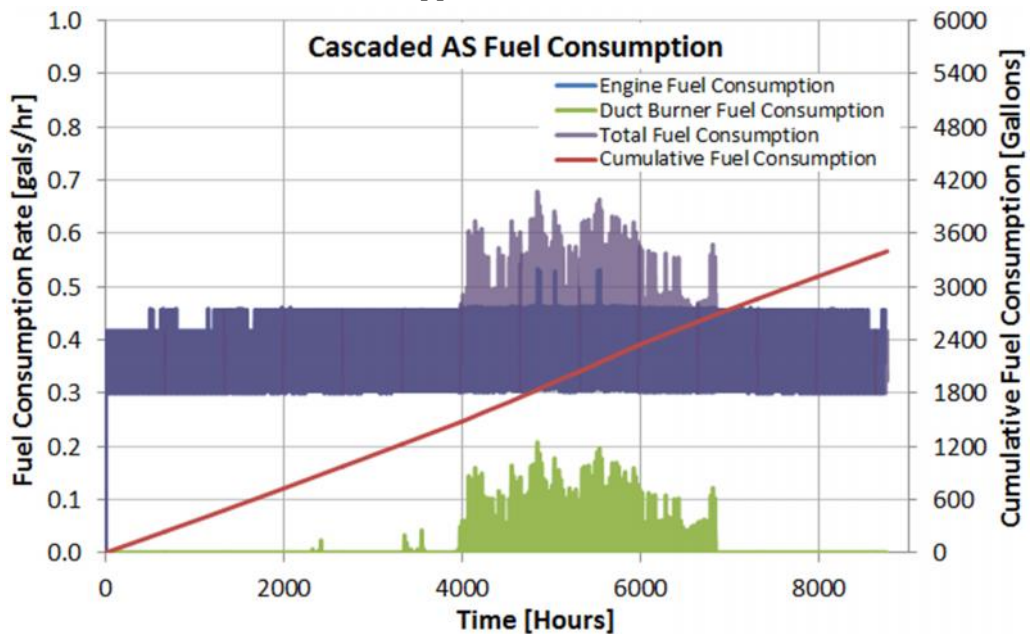
Figure 47: Cascaded AS fuel consumption for transient full year profile (DB runs mainly in the summer hours, but the engine runs with a lower fuel rate at the off-peak conditions)

73

Chapter 6: Discussion, Conclusions, & Future Work

6.1 Discussion

The three main outcomes of this study and simulation were the fuel consumption, overall weight, and physical volume for the respective system models and test cases. The results are displayed both in table and graphical format: fuel consumption results are displayed in Table 20 and Figure 48, weight comparisons are shown in Table 21 and Figure 49, and in Table 21 and Figure 50 are the volume based results. The volume results indicate that the AS's not only weigh less than the legacy system, but also fit into a smaller volumetric footprint as well. From the results it is clear that there are great potential savings in moving from the legacy system to a more efficient combined cooling and power system. The advantage at the design point was that the AS did not require nearly as much electricity, and thus a smaller Genset was used which burns fuel at a lower rate. The excess heat that the AS required was provided by the duct burner, converting fuel to heat at a much more efficient rate than what occurs with the engine. This is demonstrated by the FCC efficiency, showing how the absorption based systems convert fuel to cooling at a much higher rate. The advantage at off-design conditions is that the smaller 5 kW Genset for the AS's was running much closer to full load than the 10 kW Genset of the legacy system. The result is that the smaller engines were running more efficiently, with lower fuel consumption than the larger engine could achieve at its own lower part load ratio. The cascaded AS suffered more than the other AS's due to the higher electrical load of the supplemental VCS, but below ambient temperatures of 45°C it ran with similar advantages as the other AS's.

Table 20: Fuel consumption of system models for various simulation cases

System Model	FCC η	Result	Design Point	Worst Week	Average Week
Legacy System	0.225	Fuel Cons [Gallons]	163.2	119.8	107.3
Baseline Absorption System*	0.551	Fuel Cons [Gallons]	106	71.9	61.9
		Savings [%]	35.0%	40.0%	42.4%
Cascaded Absorption System	0.379	Fuel Cons [Gallons]	122.9	78.43	65.3
		Savings [%]	24.7%	34.5%	39.1%
MIAE Absorption System	0.525	Fuel Cons [Gallons]	107	74.1	66.3
		Savings [%]	34.4%	38.1%	38.2%

*Baseline AS is hypothetical since it does not have an anti-crystallization strategy, just for use in comparison to cascaded and MIAE AS's
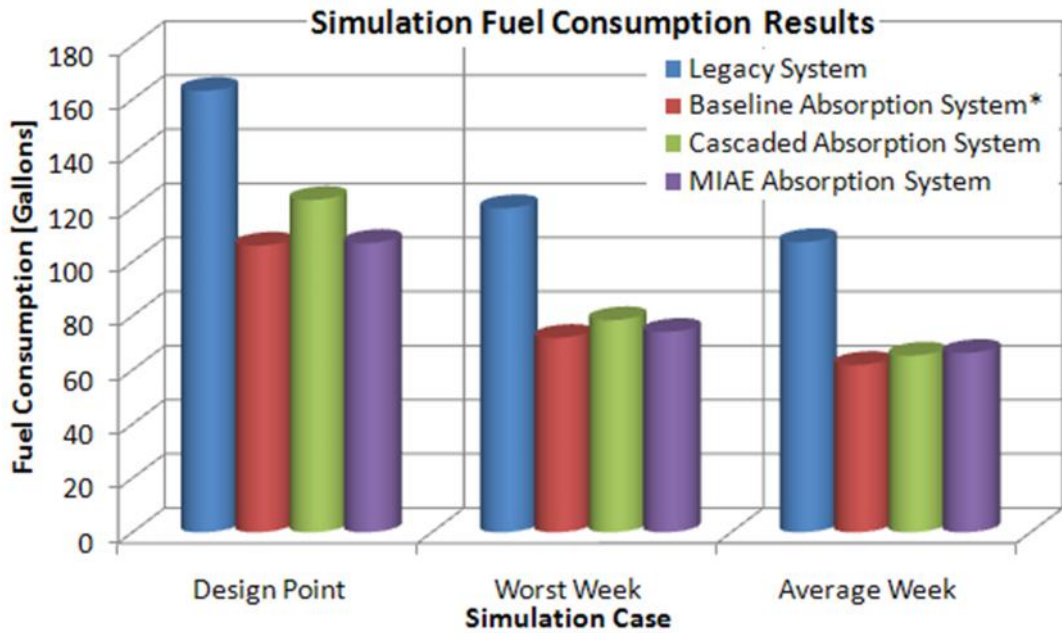
Figure 48: Fuel consumption results of simulations for system models (the legacy system clearly has greater fuel consumption for each simulation case, and the AS's have less fuel consumption that are roughly comparable)

In terms of overall weight, the greatest savings are evident when also considering the weight of fuel. This is due to the less efficient operation of the legacy system, which requires a much larger amount of fuel to be carried to fulfill the same tasks. This is true

75

even for the cascaded system, which, without fuel, weighs a little more than the legacy system due to the supplemental VCS. However, when a week of fuel is factored in, the savings become apparent. The average week was calculated using the cumulative fuel consumption for the full year divided by 52 weeks.

Table 21: Overall system weights/volumes for various models (each of the AS's have both weight and volume savings over the legacy system, especially when considering the weight and volume of the fuel for each simulation case)

System Model	Result	System w/out Fuel	Worst Week	Average Week
Legacy System	Weight [Kg]	649	1027	987
	Volume [m^3]	1.82	2.27	2.23
Baseline Absorption System*	Weight [Kg]	574	800	774
	Volume [m^3]	1.58	1.85	1.82
	Weight Savings [%]	11.6%	22.1%	21.6%
	Volume Savings [%]	13.1%	18.5%	18.1%
Cascaded Absorption System	Weight [Kg]	660	907	866
	Volume [m^3]	1.90	2.20	2.15
	Weight Savings [%]	-1.7%	11.6%	12.3%
	Volume Savings [%]	-4.4%	3.4%	3.5%
MIAE Absorption System	Weight [Kg]	594	828	803
	Volume [m^3]	1.76	2.04	2.01
	Weight Savings [%]	8.5%	19.4%	18.7%
	Volume Savings [%]	3.5%	10.4%	9.9%

*Baseline AS is hypothetical since it does not have an anti-crystallization strategy, just for use in comparison to cascaded and MIAE AS's
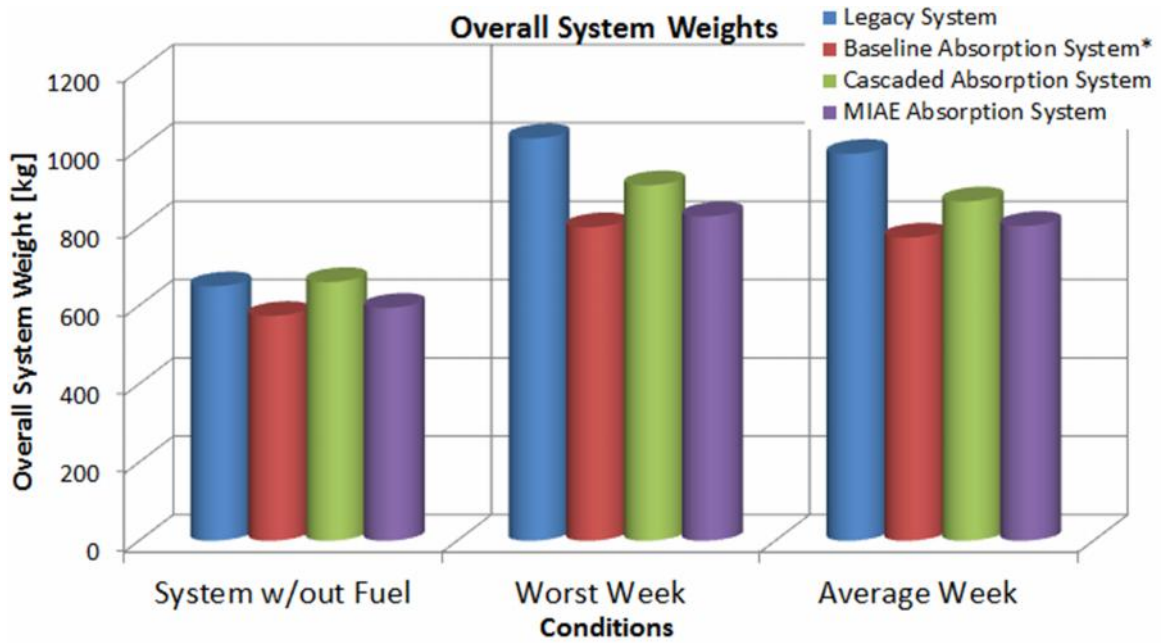
Figure 49: Overall system weights for system models and simulation conditions (the average week is made up of the full year fuel consumption and divided by 52 weeks. Due to the better performance of the AS at off-season conditions, the average week results in a lower weight)
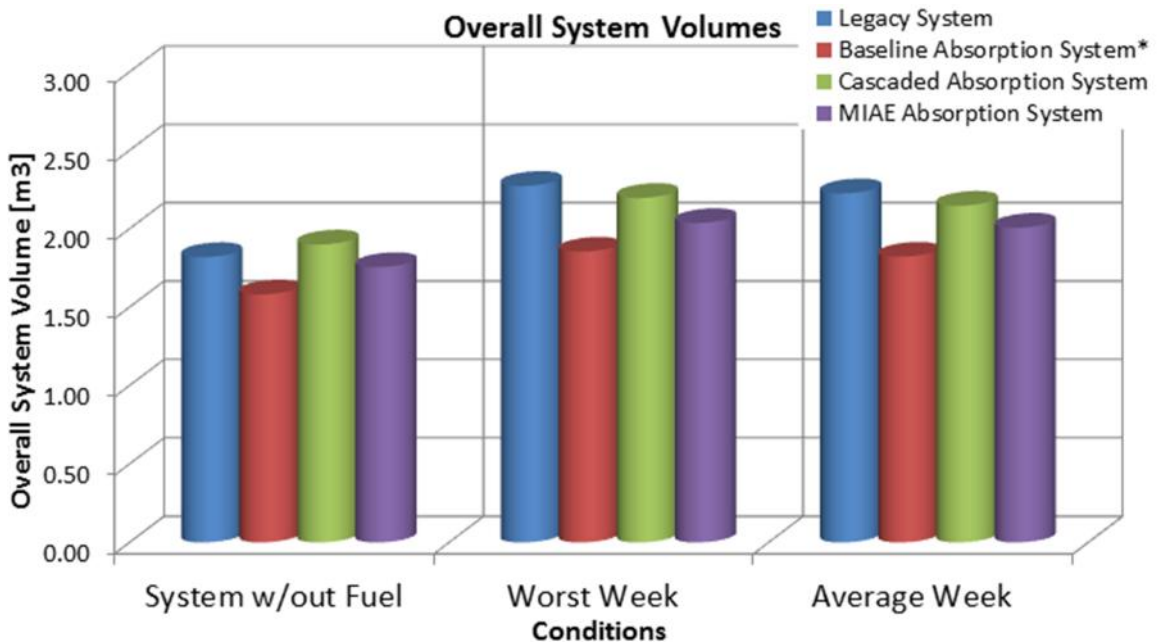
Figure 50: Overall system volumes for system models and simulation conditions (just as the case with the overall system weights, the overall system volume is less when considering the average week than for the worst week. Additionally, the volume of the AS's are reduced when considering the fuel, but not necessarily without the fuel)

The transient fuel consumption details for an AS next to the legacy system further indicate the advantages of an AS. In Figure 51 are the fuel consumption graphs for each of the investigated systems corresponding to the worst week weather profile and the transient NC load profile. Side-by-side views show a dramatic difference in continual fuel consumption efficiency in addition to cumulative amounts.

(a)

(b)

(c)

(d)
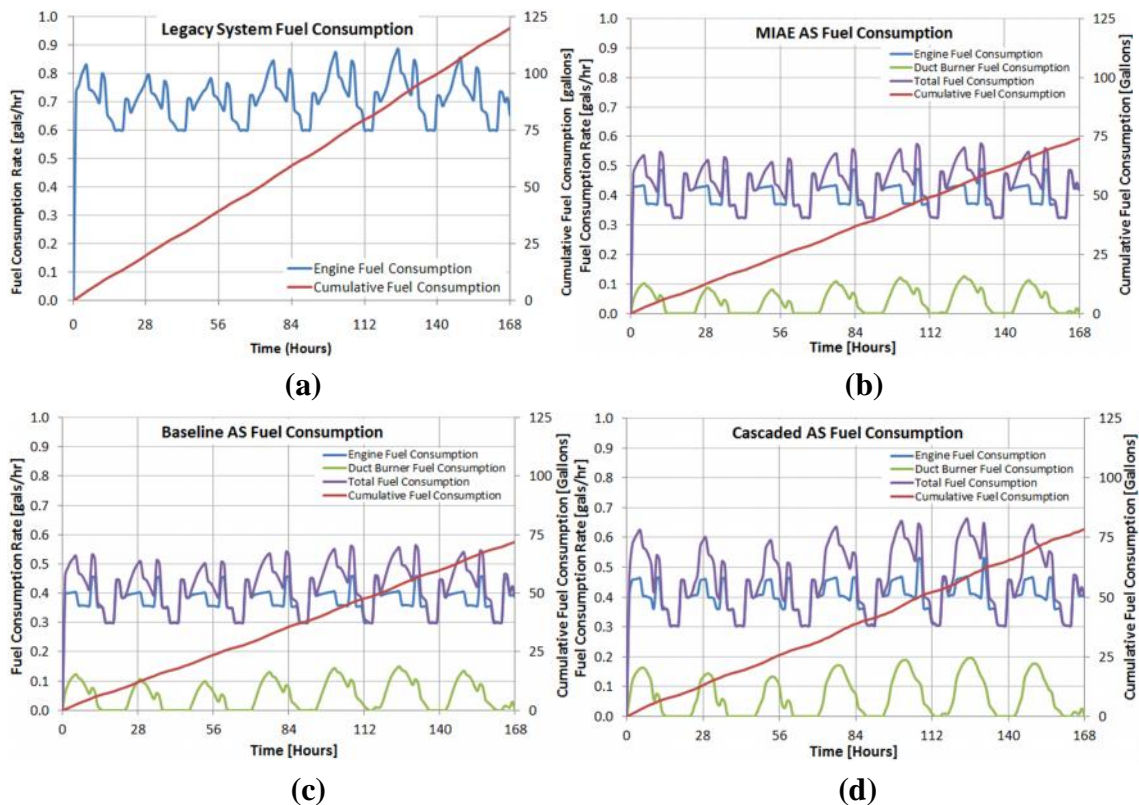
Figure 51: Week long fuel consumption of each system, (a) Legacy (b) MIAE (c) Baseline (d) Cascaded (shows the relative fuel consumption of one system to another, demonstrating that all the AS's operate with a much lower fuel rate, and result in a lower cumulative fuel consumption)

Comparison of one to the other demonstrates the remarkable difference in fuel consumption rate, especially of just the engines. It also further emphasizes the point of the efficiency in using a duct burner to provide the extra heat for a heat activated cooling

device, over providing more electricity to power a VCS to provide all the cooling. The year-long simulation was important because it demonstrated the greater potential of the AS configurations, highlighting the lower fuel consumption due to the smaller engine running at more optimal part loads as compared with the legacy system 10 kW Genset.

6.2 Conclusions

The results of this study demonstrate the efficiency advantages of moving away from conventional engine-driven VCSs toward those based on combined cooling, heat, and power. In this particular case, there is potential for at least 38% savings in fuel, a reduction of 19% on weight, and 4% physical size over the conventional legacy system which is currently in place.

Overall, this study found that the best savings and most practical option would be to use the MIAE AS configuration. The MIAE configuration addresses the crystallization issue that currently prevents AS from use in high temperature situations, while requiring less electricity than other approaches. Furthermore, it offers a reduction in weight over a typical AS, and requires less capacity from the AS evaporator than the cascaded configuration.

While the MIAE configuration holds the most potential, the cascaded configuration also provides a great alternative. This is especially true since a more common AS design could be adapted with a customized VCS to create the desired effect. Its advantage is further proved by the margin of fuel savings when comparing the various AS's. It can be seen that the cascaded configuration fuel savings are less than 4% behind the MIAE for the worst week simulation, and actually is slightly better when considering the full year

simulation. The annual improvement is because the supplemental VCS can be shut off below 45°C, resulting in a lower parasitic load than the MIAE for much of the year.

In view of this project's application, it is apparent that a migration away from inefficient configurations holds great promise. Not only are there significant cost savings, but also the reduction in fuel consumption means improving the safety of the military through less down time and less danger associated with the transport of fuel.

6.3 Future Work

Despite the advantages available from the system configurations and profiles examined, there are additional simulation profiles that could be considered, offering further realistic results and options. These would include using a less demanding profile for NC electrical load, substituting an engine component based on manufacturer data (which reports lower fuel consumption than the experimental data), and creating a more competitive system model similar to the legacy system (with the VCS providing supply air at the same temperature as the AS's supply air temperature). Additionally, the SSLC system could be re-evaluated, and some of the promising additives which were discussed could be investigated in detail for actual inclusion in a real system. These additional cases would not invalidate the results already found, but would simply give additional information about other available options. The current results are based on the design variables and objectives as they were defined for this particular study.

Pertaining to an actual physical product, a number of items require additional development. For the MIAE based AS, the MIAE unit requires further experimental testing to validate the actual capability of crystallization avoidance and the consequent

state points for the AS. In addition, the MIAE unit will need to be investigated for compatibilty with the use of air-side heat exchangers rather than the current use of liquid-liquid heat exchangers which require additional water loops. In terms of the cascaded AS, practical designs will need to be investigated for air-cooled absorber and condenser heat exchanger units. Since air-cooled heat exchanger units are not common for AS's, new designs should be investigated now that this study has shown the potential savings available for this application by switching to a CHP approach.

Appendix

The required cooling load for the space was specified as 5.275 kW. The various contributions were then backed out from this value by Kyle Gluesenkamp. This allowed for the cooling load of the space to vary with transient profiles. The space to be cooled was visually estimated from the picture in Figure 52, resulting in the volume and surface area estimates found in Table 22. These numbers were useful in estimating the contributing loads. The space to be cooled had loads associated with internal heat gains from two occupants and electrical equipment in addition to external loads associated with ventilation, infiltration, conduction, and solar gains. The infiltration flow rate was estimated as 10 CFM (~17 m^3/hr) which corresponds to the leaky end of the building envelope spectrum. Based on a total internal volume estimate of 8.5 m^3 for the space, this correlates to about 2 air changes per hour. The 10 CFM of infiltration translated to 430 Watts of infiltration load with a sensible heat factor (SHF) of 0.39.
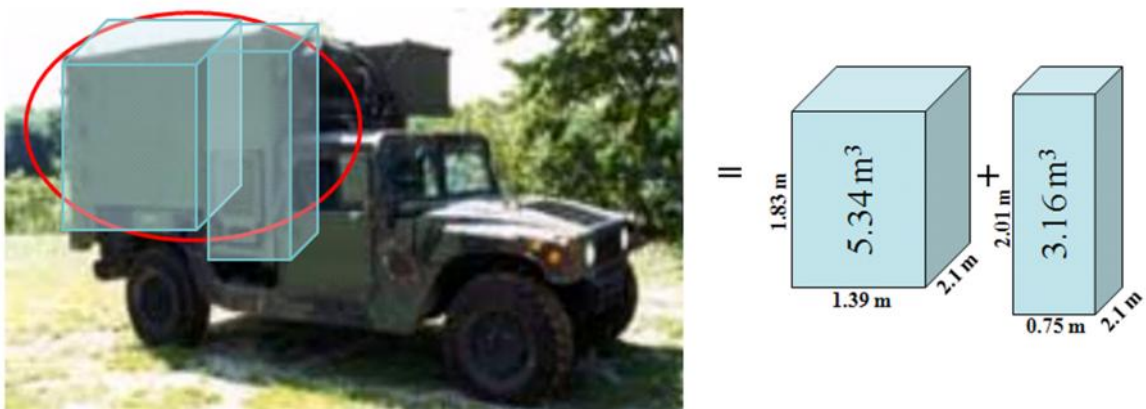

Figure 52: Visual dimensions of conditioned space (total volumetric dimensions approximated by visual estimation)

Table 22: Dimensions of conditioned space

Space dimensions:	Metric	English
Internal volume (empty)	8.5 m^3	300 ft^3
Total surface area	25.5 m^2	275 ft^2
Roof surface area	4.5 m^2	48 ft^2
Side surface area (each)	8.1 m^2	87 ft^2
Back surface area	3.8 m^2	41 ft^2
Front surface area	4.2 m^2	45 ft^2
Bottom surface area	4.9 m^2	52 ft^2

To estimate the solar and conduction loads of the space, a conductance, U value of 1 W/m^{2}K was assumed for the walls. An indoor temperature of 32.2°C and outdoor temperature of 51.7°C resulted in a 20°C temperature difference. With this temperature difference and 25 m^2 of surface area, the resulting conduction heat load alone amounted to 0.51 kW. The solar heat gain was calculated based upon 1000 W/m^2 solar insolation incident upon the structure, resulting in 4-9 kW of solar radiation varying by the position of the sun and vehicle. Without windows present, the only effect would be raising the surface temperature of the walls, therefore increasing the conduction heat load of the space. Reaching a surface temperature 20°C higher than the ambient temperature on the half of the vehicle exposed to the sun, an average temperature difference of 30°C between inside and outside brings the total conduction heat load to 0.77 kW.

The ventilation rate was eventually fixed at 45 CFM, which was more than enough for two people according to the ASHRAE standard which calls for 15-20 CFM per person. For a SHF of 0.39, each 10 CFM requires 430 W of cooling, the same as for the infiltration calculation. This brings the ventilation load to 1.575 kW.

Accounting for internal loads, the space would be occupied by two people each contributing 50 W of sensible load and 150 W of latent load, amounting to 400 W total.

Additionally, a portion of the electronic equipment powered by the Genset would be located inside of the conditioned space, contributing to the internal load. The remainder of the 5.275 kW load was ascribed to this internal equipment, resulting in 58.2% of electrical power dumped to the space. Table 23 summarizes the different contributors to the overall heat load as discussed.

Table 23: Summary of estimated loads at design conditions

		Sensible [kW]	Latent [kW]	SHF [-]		Total [kW]	
Space loads	Two occupants	0.1	0.3	0.25		0.4	
	Internal equipment	1.745	0	1.0	0.83	1.745	3.34
	Conduction + solar	0.77	0	1.0		0.77	
	Infiltration	0.17	0.26	0.39		0.43	
Ventilation loads (45 CFM)		0.74	1.19	0.39		1.93	
Sum (i.e. evaporator load)		**3.45**	**1.75**	**0.66**		**5.28**	

Based on this design point table, Eq. 6 was derived, shown again below as Eq. 46. The 0.4 kW is static based upon two occupants with 58.2% of the hotel power electrical load between 0.75 and 3 kW dumped into the space. The last section was made up of the conduction, solar, infiltration, and ventilation loads which would vary with the ambient temperature. At the design temperature of 51.7°C, these should amount to 3.13 kW, and with an outdoor temperature equivalent to the indoor set point of 32.2°C these were estimated as 0 kW. Thus, a line connecting these points on a temperature versus heat graph results in a slope of 0.1605 kW/°C.

$$Q_e[kW] = 0.4 + 0.582 * Hotel\ Power + 0.1605 * (T_{ambient} - T_{setpoint}) \quad (46)$$

The curve fits for the baseline AS's derived from EES model data described in Section 3.1, resulted in equations calculated by TableCurve 3D. The equations corresponding to Figures 16-20 are defined below in Eqs. 47-51. Correlations which resulted in both high r^2 values and a close visual match between the input values and those calculated by the equations were chosen. Equations for the cascaded AS curve fits from Section 3.2 corresponding to Figures 24-28 are displayed in Eqs. 52-56. Corresponding to the MIAE AS curve fits in Figures 30-34 from Section 3.3 are Eqs. 57-61.

Baseline COP Curve Fit Duct On

Rank 5 Eqn 318 $z=a+b/x+c/y+d/x^2+e/y^2+f/(xy)+g/x^3+h/y^3+i/(xy^2)+j/(x^2y)$

r^2=0.99976858 DF Adj r^2=0.9997589 FitStdErr=0.00039874076 Fstat=115203.67

a=2.0018284 b=-126.94693 c=-772.02726 d=3353.3601 e=89775.402

f=54686.412 g=-24055.714 h=517902.2 i=-4820897.5 j=-756518.31

$$(47)$$

Baseline COP Curve Fit Duct Off

Rank 59 Eqn 307 $z=a+bx+c/y+dx^2+e/y^2+fx/y$

r^2=0.99994202 DF Adj r^2=0.99994055 FitStdErr=0.0004860474 Fstat=817531.8

a=0.66505008 b=-0.00059158075 c=178.21048

d=9.9560202e-06 e=-13769.044 f=-3.543955

$$(48)$$

Baseline T3 Curve Fit

Rank 85 Eqn 301 $z=a+bx+cy+dx^2+ey^2+fxy$

r^2=0.99996317 DF Adj r^2=0.99996226 FitStdErr=0.10966661 Fstat=1325108.9

a=-20.069367 b=1.2491648 c=-0.0069860172

d=0.013429214 e=3.1215508e-05 f=0.0010979192

$$(49)$$

Parastic Power Duct On

Rank 322 Eqn 1 $z=a+bx+cy$

r^2=0.99992864 DF Adj r^2=0.99992792 FitStdErr=0.75946749 Fstat=2080835.7

a=-57.20974 b=11.44622

c=0.19474679

$$(50)$$

85

Parasitic Power Duct Off
Rank 44 Eqn 301 $z=a+bx+cy+dx^2+ey^2+fxy$
$r^2=0.99993117$ DF Adj $r^2=0.99992996$ FitStdErr=0.034372866 Fstat=999479.92
a=342.81071 b=-0.22011357 c=0.14832681
d=0.009900928 e=-7.436287e-06 f=-0.0010098053

(51)

Cascaded system COP curve fit
Rank 7 Eqn 318 $z=a+b/x+c/y+d/x^2+e/y^2+f/(xy)+g/x^3+h/y^3+i/(xy^2)+j/(x^2y)$
$r^2=0.99986812$ DF Adj $r^2=0.99986258$ FitStdErr=0.00034900793 Fstat=201340.31
a=1.2553452 b=-64.388 c=-408.88103 d=1808.0733 e=38490.993
f=32892.554 g=-12168.503 h=2263392.4 i=-3038439.2 j=-461664.59

(52)

Cascaded System T3 Curve Fit Duct On
Rank 204 Eqn 301 $z=a+bx+cy+dx^2+ey^2+fxy$
$r^2=0.99998413$ DF Adj $r^2=0.99998373$ FitStdErr=0.069265842 Fstat=3061393.6
a=-54.972853 b=2.3945889 c=0.055234157
d=0.0037459964 e=8.5045352e-07 f=8.5484589e-05

(53)

Cascaded System Parasitic Power Duct On
Rank 349 Eqn 1 $z=a+bx+cy$
$r^2=0.99991556$ DF Adj $r^2=0.99991452$ FitStdErr=0.65290527 Fstat=1456499.5
a=84.336841 b=11.360623
c=0.18883167

(54)

Cascaded system parasitic power duct off
Rank 42 Eqn 301 $z=a+bx+cy+dx^2+ey^2+fxy$
$r^2=0.99993333$ DF Adj $r^2=0.99993169$ FitStdErr=0.048603651 Fstat=731969.2
a=477.78956 b=-0.29490683 c=0.22045459
d=0.011495023 e=-5.8985528e-06 f=-0.0017183108

(55)

Cascaded System Qe Duct on
Rank 356 Eqn 11 $z=a+bx+c/y$
$r^2=0.99913867$ DF Adj $r^2=0.99912812$ FitStdErr=0.034499996 Fstat=142678.94
a=0.20287142 b=0.17763697
c=-1663.3053

(56)

MIAE COP Curve Fit Duct On
Rank 9 Eqn 318 $z=a+b/x+c/y+d/x^2+e/y^2+f/(xy)+g/x^3+h/y^3+i/(xy^2)+j/(x^2y)$
$r^2=0.99948277$ DF Adj $r^2=0.99946113$ FitStdErr=0.00039616826 Fstat=51530.042
a=1.4886296 b=-78.754896 c=-546.58864 d=2019.6039 e=58032.626
f=40750.589 g=-10700.044 h=1370194.6 i=-3496316.8 j=-626026.14

(57)

MIAAE COP Curve Fit Duct OFF

Rank 117 Eqn 303 $z = a + b/x + cy + d/x^2 + ey^2 + fy/x$

$r^2 = 0.9994166$ DF Adj $r^2 = 0.9994022$ FitStdErr $= 0.001661576$ Fstat $= 83598.91$

$a = -0.45067891$ $b = 38.389051$ $c = 0.0018112295$

$d = -300.19194$ $e = -1.0962492e{-}06$ $f = -0.023335274$

$$(58)$$

MIAE T3 Curve Fit

Rank 214 Eqn 16 $z = a + bx + cx^2 + dy$

$r^2 = 0.99998347$ DF Adj $r^2 = 0.9999832$ FitStdErr $= 0.064984139$ Fstat $= 4961526$

$a = -32.665754$ $b = 1.9696013$

$c = 0.0065541288$ $d = 0.044671998$

$$(59)$$

MIAE Parasitic Power Curve Fit Duct On

Rank 240 Eqn 16 $z = a + bx + cx^2 + dy$

$r^2 = 0.99998365$ DF Adj $r^2 = 0.99998338$ FitStdErr $= 0.2885317$ Fstat $= 5015460.2$

$a = 286.5189$ $b = 13.200439$

$c = -0.021303807$ $d = 0.18830163$

$$(60)$$

MIAE Parastic Power Curve Fit Duct Off

Rank 354 Eqn 16 $z = a + bx + cx^2 + dy$

$r^2 = 0.99447694$ DF Adj $r^2 = 0.99438677$ FitStdErr $= 0.48801027$ Fstat $= 14764.855$

$a = 744.68245$ $b = -1.2638488$

$c = 0.014819701$ $d = 0.17019977$

$$(61)$$

Bibliography

[1] NPR Staff, "*Among the Costs of War: Billions A Year in A.C.?*" All Things Considered, June 25, 2011 <http://www.npr.org/2011/06/25/137414737/among-the-costs-of-war-20b-in-air-conditioning?ps=cprs>

[2] Colson, C. M, and M. H Nehrir. "Evaluating the Benefits of a Hybrid Solid Oxide Fuel Cell Combined Heat and Power Plant for Energy Sustainability and Emissions Avoidance." *IEEE Transactions on Energy Conversion* 26.1 (2011): 140–148.

[3] Mago, Pedro J., Anna Hueffed, and Louay M. Chamra. "Analysis and Optimization of the Use of CHP–ORC Systems for Small Commercial Buildings." *Energy and Buildings* 42.9 (2010): 1491–1498. Web. 21 Mar. 2012.

[4] Deng, J., R.Z. Wang, and G.Y. Han. "A Review of Thermally Activated Cooling Technologies for Combined Cooling, Heating and Power Systems." *Progress in Energy and Combustion Science* (2010) 1-32

[5] Barberis, Francesco. "Applications of Absorption Chillers", in *International Sorption Heat Pump Conference* (2011) Padua, Italy, April 5-7, 2011.

[6] Herold, K. E., Radermacher, R. and Klein, S. A. *Absorption Chillers and Heat Pumps,* Boca Raton, Fla.: CRC Press, 1996.

[7] Zogg, R. Westphalen, D. "Developing Air-Cooled LiBr Absorption for Light Commercial Heat and Power Applications." *HVAC&R Research Special Issue* 12.3b (2006) 731-747.

[8] Cristiani, J. M. "3kW Tactical Quiet Generator Fuel Consumption and Load Profile," U.S. Army CERDEC (2010). Unpublished Raw data.

[9] "3kW Tactical Quiet Generator (TQG) Set 60Hz." DRS Power Solutions. <http://www.drspowersolutions.com/en/home/OurProducts/GeneratorSets/MEP-831/Specification.aspx> April 5 2012.

[10] "L70V Air-cooled, 4-Cycle, Single Cylinder, Industrial Engine." Yanmar. <http://us.yanmar.com/products/industrial-engines/air-cooled/epa-certified/l-v-series/l70v/> April 3, 2012.

[11] Remund, J. and Kunz, S. Meteonorm Version 5. METEOTEST, Bern, Switzerland. 2003. <www.Meteotest.com>

[12] Klein, S. A. Alvarado, F. L. Engineering Equation Solver (EES), F-Chart Software, WI, USA, 1997.

[13] Klein, S. A. Backman, W. TRNSYS 17, a TRaNsient SYstem Simulation program, Solar Energy Laboratory, University of Wisconsin, Madison, WI, USA, 2010.

[14] SYSTAT Software Inc. TableCurve 2D 5.01: Automated Curve Fitting & Equation Discovery, Chicago, IL. 2002.

[15] "10kW Tactical Quiet Generator (TQG) Set 60Hz." DRS Power Solutions. September 2010. <http://www.drspowersolutions.com/en/home/OurProducts/GeneratorSets/MEP-803/Specifications.aspx>

[16] "AirRover ULCR24BA" AirRover Inc. May 2011. <http://www.airrover.com/products.php?item=66&sub=performance>

[17] Gluesenkamp, K., Horvath, Christopher, Radermacher, R. and Hwang, Y. "Air-Cooled, Single Effect, Waste Heat-Driven Water/Libr Absorption System For High Ambient Temperatures", in *International Sorption Heat Pump Conference*, (2011) Padua, Italy, April 5-7, 2011.

[18] Boryta, D. A. "Solubility of lithium bromide in water between -50.deg. and +100.deg. (45 to 70% lithium bromide)', *Journal of Chemical & Engineering Data,* 15(1), (1970) 142-144.

[19] Zogg, R. A., Feng, M. Y. and Westphalen, D. *Distributed Energy Program Report: Guide to Developing Air-Cooled LiBr Absorption for Combined Heat and Power Applications*, (2005) US Department of Energy, Energy Efficiency and Renewable Energy.

[20] Wight, S.E., Yoshinaka, T., LeDrew, B. A. D'Orsi, N. C. (Concepts ETI). 2000 NOV. "The Efficiency Limits of Water Vapor Compressors," Final Report. Arlington (VA): Air-Conditioning and Refrigeration Institute (ARTI). Springfield, VA, ARTI-21CR/605-10010-01, DE-FC05-99OR22674. 260. Available by U.S. Department of Commerce.

[21] Gluesenkamp, K., Radermacher, R. and Hwang, Y. (2011) "Crystallization Inhibitors For Water/Libr Absorption Chillers", *International Sorption Heat Pump Conference*, Padua, Italy, April 5-7, 2011.

[22] Okano, T., Asawa, Y., Fujimoto, M., Nishiyama, N. and Sanai, Y. (1994) 'Development of an air-cooled absorption refrigerating machine using a new working fluid', in *International Absorption Heat Pump Conference*, New Orleans, LA, USA

[23] Tongu, S., Makino, Y., Ohnishi, K. and Nakatsugawa, S. "Practical operating of small-sized air-cooled double-effect absorption chiller-heater by using lithium bromide and aqueous [sic]", in *International Absorption Heat Pump Conference*, (1994) New Orleans, LA, USA, ASME.

[24] Bourouis, M., Vallès, M., Medrano, M. and Coronas, A. "Absorption of water vapour in the falling film of water-(LiBr + LiI + LiNO3 + LiCl) in a vertical tube at air-cooling thermal conditions", *International Journal of Thermal Sciences,* 44(5), (2005) 491-498.

[25] Reimann, R. C. and Biermann, W. J. "Phase III Final Report: Development of a single-family absorption chiller for use in solar heating and cooling system", (1984) *Carrier Corporation*.

[26] Yazaki Corporation, Japanese Patent 2000-319646, *Absorbing Solution for Absorption Refrigerating Machine and Absorption Refrigerating Machine*. (2000)

[27] Schroder, A. Rotartica Product Description. <http://andyschroder.com/rotartica.html> Web. February 22, 2011.

[28] "MSR-DC 12VDC" Wayne Combustion Systems. September 2010, <http://www.waynecombustion.com/store/c-9-oil-burners.aspx>

[29] "Fans & Blowers." Surplus Sales of Nebraska. April 10, 2011, <http://www.surplussales.com/fans-blowers/FansBlow-3.html>

[30] "8-inch 110vac 500CFM In-Line Duct Fan" Suncourt Inc. April 10, 2011, <http://www.rockler.com/product.cfm?page=20039&utm_source=Nextag&utm_medium=CSE&utm_campaign=V9124&utm_term=SmartHome>

[31] "10-inch 110vac 650cfm In-Line Duct Boosterfan." Suncourt Inc. April 10, 2011, <http://www.smarthome.com/3013/10-Inch-110VAC-650CFM-In-Line-Duct-Fan-DB210/p.aspx>

[32] "AC Tubeaxal Fan, W2E250-HJ32-01." EBMPAPST. May 12, 2011, <http://www.alliedelec.com/search/productdetail.aspx?SKU=6002500#tab=Specs>

[33] "Grundfos Alpha 15-55F/LC Circulator Pump." Grundfos. May 12, 2011, <http://www.pexuniverse.com/grundfos-alpha-15-55f-lc-circulator-pump-w-ifc-1-6hp-115v>

[34] SYSTAT Software Inc. "TableCurve 3D 4.0". Chicago, IL, 2002.

[35] ASHRAE, ASHRAE handbook-systems and equipment, 2000, Chapter 34.

[36] "Grundfos UPS 26-99 BFC Bronze Recirculation Pump." Grundfos. May 12, 2011, <http://www.faucetdirect.com/grundfos-ups-26-99-bfc-bronze-recirculation-pump-with-maximum-power-input-197w-230-degree-max-temperature-range-oval-valve/p1333310>

[37] "Grundfos, UPS15-55SFC 3-Speed Stainless Steel Circulator Pump." Grundfos. May 12, 2011, <http://www.pexuniverse.com/grundfos-ups15-55sfc%20super%20brute-circulator-pump-59896773>

[38] "Grundfos, UP 15-42 Circulator Pump" Grundfos. April 6, 2012, <http://www.pexuniverse.com/grundfos-up15-42fr-circulator-pump-59896167>

[39] "Generator Set Technical Data Sheet , GS Model GS8DE." Lister Petter. September 2005.

[40] Broad Air Conditioning, "Broad X Non-Electric Chiller - Model Selection and Design Manual" September 2010.

[41] "5kW Tactical Quiet Generator (TQG) Set 60Hz." DRS Power Solutions. <http://www.drspowersolutions.com/en/home/OurProducts/GeneratorSets/MEP-802/5kWTQGSpec.aspx>April 3, 2012.

[42] Center for Environmental Energy Engineering. CoilDesigner 3.5 Beta. University of Maryland, College Park, MD. USA. 2011.

[43] "Soleus LX-140 14,000 BTU Portable Air Conditioner." Soleus Air. June 29, 2011, <http://www.air-n-water.com/product/LX-140.html>